Journal of Sustainable Development of Smart Energy Networks

https://www.sdewes.org/jsdsen

Year 2027, Volume 2, Issue 1, 2030733

Original Research Article

Techno-Economic Assessment of Green Hydrogen, Carbon Capture and Synthetic Natural Gas as Decarbonization Options for a Steel Hot Rolling Mill in Austria

***Mikel Olaciregui-Segura*[*1], *Anton Beck*[1], *Christoph Zauner*[1]**

[1]Center for Energy, AIT Austrian Institute of Technology GmbH, Vienna, Austria

e--mail: mikel.olaciregui-segura@ait.ac.at

Cite as: Olaciregui-Segura, M., Beck, A., Zauner, C., Techno-Economic Assessment of Green Hydrogen, Carbon Capture and Synthetic Natural Gas as Decarbonization Options for a Steel Hot Rolling Mill in Austria, J. sustain. dev. smart. en. net., 2(1), 2030733, 2027, DOI: https://doi.org/10.13044/j.sdsen.d3.0733

ABSTRACT

Hot rolling mills for steel processing are an energy-intensive and notably hard-to-abate industry. Previous studies have not explicitly modelled the interaction between the different technologies that potentially make up the decarbonized energy supply system of a steel rolling mill, nor considered potential limitations of electrical grid infrastructure. The combination of additional capital and operational expenses together with infrastructural limitations potentially makes deep decarbonization of such an industrial energy system economically unfeasible. In this paper, we present a complete model of a hot rolling mill in Austria with two decarbonization routes, namely green hydrogen and synthetic natural gas with carbon capture, and we use MILP optimization to derive the least-cost design and operation of the energy system under three power grid capacity scenarios and a choice of different technologies. We find a 124~166% increase in the levelized cost of heat for the hydrogen route and of 187~231% for the synthetic natural gas route, depending on power grid capacity. The results highlight the crucial role of the electrical grid in providing flexibility and confirm that, under current and-near future techno-economic conditions, a major reduction in carbon emissions from the steel processing sector is only possible with significant policy support.

KEYWORDS

Steel rolling, Reheating furnace, Decarbonization, Green hydrogen, Carbon capture, Synthetic natural gas, Mixed-integer linear optimization.

INTRODUCTION

The steel industry is one of the technological pillars of the modern world. In 2024, more than 1,740 million tons of finished steel products were produced worldwide [1]. The steel industry is energy-intensive , and most of its growth has been based on fossil fuels, resulting in 1.92 tons of carbon dioxide (CO_2) emissions per ton of steel produced [2]. However, as governments and businesses commit to a net-zero horizon that requires avoiding most emissions of climate-change-inducing greenhouse gases, it is apparent that new energy systems are required to power the production and processing of steel.

* Corresponding author

High-temperature process heat in hot rolling

High-temperature process heat is among the most challenging industrial end-uses to decarbonize because it combines high thermal power density, tight temperature–time specifications, and product-quality sensitivities that depend on furnace atmosphere and heat-transfer factors. This is particularly true for steel reheating furnaces in hot rolling mills (e.g., walking-beam and pusher furnaces), which 2.0~2.4 GJ/t of finished product [3], and where slabs are typically heated to >1100 °C (often ~1250 °C) with strict uniformity requirements to ensure stable rolling, avoid defects, and minimize yield losses through oxidation-related scaling [4]. Data compiled by the European Commission highlights that this downstream step remains a nontrivial fraction of total CO_2 emissions at around 0.13 tCO_2 per ton of product (cf. 1.29 tCO_2/t for blast furnaces), and it motivates the need to evaluate viable decarbonization alternatives at the process level, not only at the level of upstream steelmaking routes [5].

Decarbonization options for steel reheating and hot rolling

These high temperatures make it infeasible to decarbonize reheating furnaces through technologies like high-temperature heat pumps (HTHPs), which are commonly proposed in other energy-intensive, but lower-temperature processes [4]. Recent literature converges on two primary pathways for reheating-furnace decarbonization: (i) direct electrification and (ii) fuel substitution with green hydrogen (i.e. hydrogen produced from renewable electricity) [6]. A third pathway, (iii) a closed carbon loop with carbon capture and synthetic natural gas (SNG) (produced from captured CO_2 and green H_2 via methanation) offers process compatibility with existing furnace infrastructure but adds conversion steps and auxiliary units.

Direct electrification. Direct electrification eliminates combustion emissions at the point of use and can be highly efficient, but its application to large, continuous reheating furnaces is subject to important practical constraints. Replacing fuel burners with electric heating removes the flue-gas stream that supports heat recovery and affects convective mixing, meaning that furnace flow and heat-integration concepts may need to be substantially redesigned to maintain productivity and temperature uniformity [4]. Major technologies for direct electrification include resistive heaters, induction coils and plasma torches [7]. In the present study, resistive heating was examined but found unsuitable for the larger furnaces because its heat density is insufficient. Induction heating was also excluded, as it is not compatible with the site-specific products due to spatial constraints and their inhomogeneous shapes. Plasma torches, by contrast, offer a burner-like electrification concept with high power density and a hot gaseous heat-transfer medium, making them a promising option for future applications. However, because they currently remain at a relatively low technology readiness level and still face challenges related to efficiency, heat transfer, NOx formation, product quality, and maintenance, they were not included in the present study either.

Fuel substitution with green hydrogen. Hydrogen (H_2) combustion is often positioned as a relatively straightforward retrofit option because it can retain established burner–furnace architectures. High-temperature process-heat reviews note that steel reheating furnaces can technically be converted to hydrogen and that pilot/industrial deployments are approaching high readiness levels (often framed as TRL ~8–9), while also emphasizing that feasibility hinges on site constraints and available infrastructure [4]. Industrial burner development for reheating furnaces has demonstrated stable operation up to 100% H_2 with low-NO_x concepts at typical furnace temperatures, supporting the practical plausibility of hydrogen retrofits [8].

However, hydrogen shifts the decarbonization challenge upstream: the overall emissions benefit depends on the electricity mix and the availability of renewable power for electrolysis, purchase of externally produced hydrogen (via truck or pipeline), or both. In a detailed hot-

rolling reheating-furnace case study comparing natural gas, electrification, hydrogen/air, and hydrogen/oxygen concepts under different European grid mixes, the CO_2 reduction potential was shown to be highly sensitive to the carbon intensity of electricity supply and the pace of grid greening [6]. As a result, hydrogen-based decarbonization cannot be assessed independently of power-system boundary conditions—particularly in contexts where industrial electrification competes for limited renewable electricity [4, 9].

Fuel substitution of hydrogen in place of natural gas causes changes in the reheating furnace atmosphere, with a notable reduction in CO_2 and increase in water vapour (H_2O) [10]. Although industrial-scale tests of hydrogen-combustion atmospheres are still scarce, several laboratory-scale studies have been carried out to investigate the potential effects that the different chemical composition and heat transfer characteristics may have on product quality. Scaling is a major product quality concern in hot rolled products as it causes surface defects, reduces the process yield and complicates downstream surface treatments [11]. A recent study found a moderate increase in scaling in the hydrogen-air atmosphere [12]. An earlier study showed that the differences in scaling are dependent on the specific grade of steel being reheated, however [13]. Although experiments are ongoing, a CO_2-poor atmosphere could also induce decarburization issues, with implications for surface hardness and long-term fatigue [14]. The combination of changes in scaling and decarburization effects implies that a pure hydrogen fuel might not be a one-size-fits-all solution and that other alternatives should be investigated for at least some steel grades.

Fuel substitution with carbon capture and SNG. An alternative that requires minimal process modifications is to continue using methane gas (CH_4) as fuel while making the system near-carbon-neutral via CO_2 capture and utilization: CO_2 is captured from the flue gas and methanated with green hydrogen to form SNG, which is recycled as furnace fuel. Pilot demonstrations show that high capture and conversion performance are technically achievable, particularly when heat and material integration are leveraged to reduce auxiliary energy demand [15]. Process-integration studies of power-to-SNG chains further quantify how overall efficiency depends strongly on electrolysis type (steam electrolysis vs co-electrolysis), operating pressure, and heat integration between (exothermic) methanation and heat demands [16].

Nevertheless, these loops add substantial CAPEX and OPEX (capture, methanation and additional hydrogen production), and they incur an efficiency penalty through additional conversion steps. In a dedicated MILP optimization of a steel hot rolling mill, SNG produced via CO_2 capture and methanation was consistently more expensive than direct hydrogen across electricity-price scenarios, even though SNG offers storage and infrastructure compatibility advantages [17]. Still, its high compatibility with existing production processes makes it a worthwhile option to consider in feasibility studies.

Techno-economic assessment studies using MILP

Because technology choice depends on discrete design decisions and time-dependent operation, recent work increasingly uses optimization-based approaches to compare decarbonization pathways under realistic constraints.

Mixed-integer linear programming (MILP) enables joint optimization of (i) discrete technology selection, (ii) capacity sizing, and (iii) time-resolved dispatch under variable production demands, energy prices and infrastructure constraints. In the hot rolling context, a recent MILP study comparing on-site hydrogen and on-site SNG under dynamic electricity pricing demonstrates that exploiting price variability via flexible operation and storage can substantially reduce levelized costs of energy (LCoE) relative to flat-price assumptions; it also shows that optimal electrolyser selection shifts with electricity-price level due to efficiency–CAPEX trade-offs [17].

Studies from other sectors that also require high-temperature process heat show that deep decarbonization is often achieved via hybrid solutions, and that the last step toward near-zero emissions can be disproportionately expensive. In glass-furnace techno-economic optimization, partial electrification combined with on-site renewables and storage can achieve moderate abatement at modest cost increases, whereas pushing toward very high abatement levels requires substantially larger investments in storage or hydrogen infrastructure [18]. Multi-stage MILP optimization in cement similarly indicates that combining multiple measures (e.g., alternative energy supply, capture, and integration) can deliver major emissions reductions while highlighting the importance of phased investments and policy incentives for economic viability [19]. Cluster-level MILP studies in high-temperature chemical sectors show that the availability of CO_2 transport/storage and power infrastructure can dominate outcomes and that integration across units can reduce costs and emissions compared to isolated decarbonization measures [20]. Collectively, these findings support the expectation that hot rolling mills will benefit from evaluating portfolios of decarbonization options and from explicitly representing time-varying operation and infrastructure constraints, in order to best quantify the business impact of deep decarbonization targets.

Research gaps and motivation for this study

Much of the peer-reviewed literature for decarbonization in the iron and steel sector is dedicated to the production of raw steel, while the studies on downstream processing of steel products remain comparatively sparse. The most relevant techno-economic assessment study is the doctoral dissertation by Löffler [21], recently expanded upon in a paper by Zabik, Birkelbach et al. [17]. They apply a MILP methodology to optimize the technology choice, capacity sizing and operation of a decarbonized energy supply system for a hot rolling mill in Austria, and carry out a detailed comparison of the LCoE of a hydrogen- vs SNG-based system under a variety of different energy price scenarios. There are however three additional elements not explored in their case study, and which our present work includes to provide a fuller understanding. These are namely different electrical grid capacity scenarios, which influence the planning of major investments; inclusion of onsite PV and wind power generation in the mix; explicit modelling of carbon capture subsystems; and hybrid solutions combining the advantages of more than one technology.

On the one hand, the strong increase in electricity demand expected from onsite production of green hydrogen calls for an evaluation of different grid connection regimes, especially given the structural bottlenecks that the Austrian power grid faces in the near future [22]. If a substantial part of the additional demand is satisfied through onsite renewables, grid feed-in dynamic of excess power in times of high generation and/or low process demand also need to be considered. The development of plans for investments in the grid is in turn influenced by the demands expected from electricity consumers in general and energy-intensive industries in particular. Consequently, the present work can provide insights into the interrelation of industrial planning and grid conditions and thus be helpful to decisionmakers on both sides.

On the other hand, the previous study only considers electricity supply from the general grid. The present work also introduces the possibility of building solar PV an wind power generation connected directly to the plant, which potentially decreases dependency on the grid but also requires consideration of seasonal variations in generation potential which do not necessarily correlate to variations in process heat demand. The optimal electrical mix for each scenario is calculated trough a representative period based approach.

In addition, their study simplifies the carbon looping subsystem as a per-unit carbon capture cost; an explicit modelling of the available technologies for carbon capture would enable an optimization of the design of the carbon capture subsystem as well as of the heat integration between its energy heat demands and the waste heat from the furnaces and the methanation reaction on the other.

Finally, their model presents a conventional binary choice between electrolysis technologies, while this work allows for more general (albeit potentially less feasible in practice) hybrid solutions in the electrolysis, carbon capture and methanation subsystems that implement more than one technology in order to take advantage of each one's relative strengths.

By examining the optimal decarbonized system under different grid connection regimes, explicitly modelling and optimizing the closed carbon loop subsystem and allowing for multi-technology solutions while simplifying the energy price conditions, the present work aims to complement previous case studies and provide a fuller picture of the challenges and opportunities the steel processing industry faces on its road to the net-zero economy.

MODEL AND METHODS

In this section, a MILP model of a steel hot rolling mill in Austria is developed as a collection of subsystems, with the combined superstructure shown in Figure 1. The objective function and the constraints are defined as linear combinations of non-negative real and binary decision variables, which model both the design and operation of the decarbonized energy system. The superstructure allows for hybrid solutions, possibly combining different technologies in the same subsystem.

The MILP approach was chosen because it is a well-established method for energy system expansion planning and allows the simultaneous optimization of design and operation. It remains computationally efficient even for complex system configurations and guarantees a global optimum as long as the problem is formulated linearly. This makes it particularly suitable for system-level planning studies. Its main limitation is that nonlinear effects, especially part-load behaviour of individual technologies, can only be represented through piecewise-linear approximations. Moreover, nonconvex functions would require introduction of additional binary variables and thus would make the model much harder to trace. Thus, in this work we aimed for simple linear constraints and refrained from piecewise approximations.

The available routes for decarbonization were narrowed down by a preliminary feasibility review. The industrial partner ruled out direct electrification for a variety of reasons: resistive heating might pose difficulties with achieving the desired temperatures in the existing furnace design due to low heating density; the thickness of some pieces makes induction unsuitable for this case study; and plasma burners are not at a sufficiently high TRL yet. Furthermore, the internal tests on the product quality impact of the hydrogen combustion atmosphere are still inconclusive, and therefore the potentially more expensive, but production-wise less problematic CC+SNG route is also investigated as an alternative to the pure-H_2 route.

For computational tractability, the whole year is modelled by taking a randomly selected sample $\mathcal{P}$ of 22 days p (one-sixteenth of the year), each composed of 24 1-hour steps t:

$$t \in \mathcal{T} = \{0, \dots, 23\} \tag{1}$$

$$p \in \mathcal{P} = \{31,34,47,71,136,151,153,164,183,185,187,227,\\ 245,257,262,268,272,283,300,304,347,350\} \tag{2}$$

An analysis of the trade-off between computational tractability and robustness of results was conducted (see Appendix) and yielded the chosen sample size of 22 days as a number that produces sub-5% uncertainty in the objective function value across 13 realizations while keeping computation time low enough to enable quick iteration over different scenarios and parameter values. The choice of 1-hour steps, meanwhile, is based on the time resolution of the data for process heat and electricity demand that the industrial partner made available for the study.

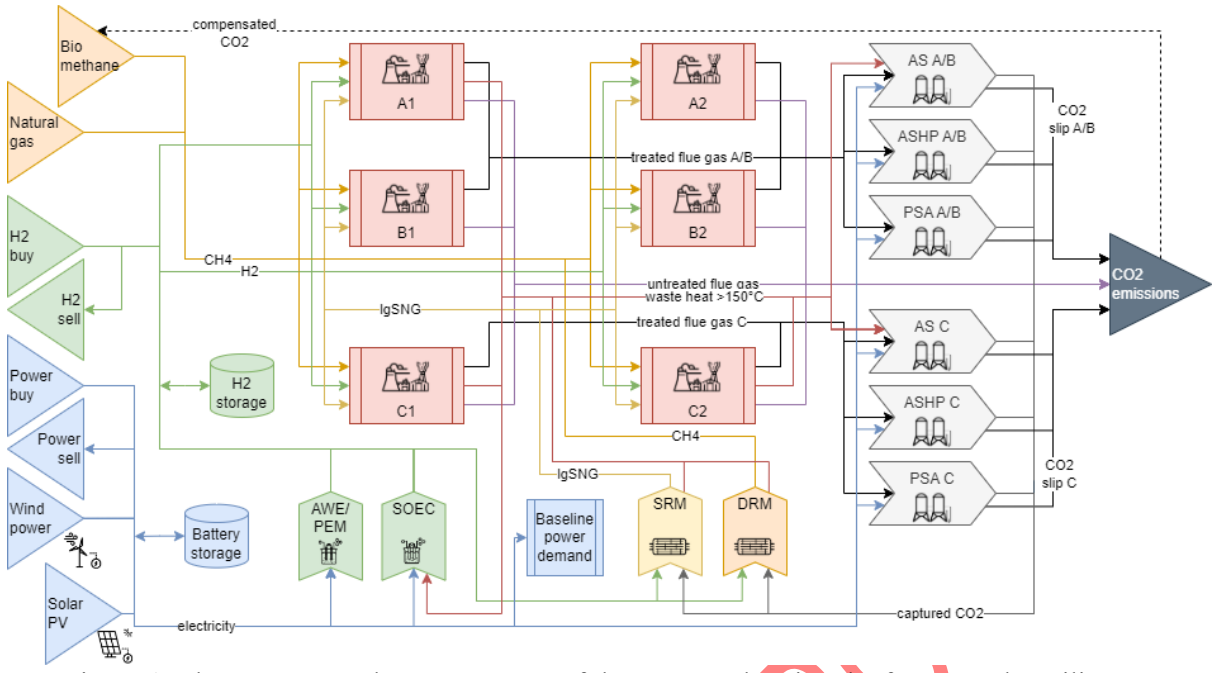

Figure 1. The most general superstructure of the system, showing the furnaces, the utility connections and the energy conversion units, as well as all the relevant flows of energy and mass, as described through the "Model and Methods" section. Red: the six furnaces with their fuel inputs, energy outputs and carbon outputs. Blue: the power subsystem consisting of grid connections (purchase and feed-in), onsite renewables (hydro, wind and/or solar PV) and a possible battery storage. Green: the hydrogen subsystem, which exists both in the H2 and CC+SNG routes, and consists of the external connections (purchase and feed-in), the available electrolysers (AWE/PEM and/or SOEC), and a possible H2 tank storage. Gray: the carbon capture subsystem, consisting of the available CC technologies (AS, ASHP and PSA) for both the A/B and C groups of furnaces, internal connections for CO2 utilization, and accounting of direct emissions. Orange and yellow: the methanation subsystem with the two available reactor technologies (OSM and/or TSM), as well as the natural gas and biomethane purchase connections. The latter two subsystems are only needed in the CC+SNG route.

Industrial process

The plant consists of several reheating furnaces, of which six are considered in this study. They will be referred to as furnaces furn = A1, A2, B1, B2, C1 and C2. Furnace A1 is used for reheating steel billets from room temperature to forming temperature, and furnace A2 for keeping them hot after rolling. Later, the steel pieces are further processed in one of two heat treatment lines: either at furnaces B1 and B2, which are co-located with furnaces A1 and A2; or at furnaces C1 and C2, which are located in a separate building.

Time series of temperature and load were provided by the plant for all furnaces, with a duration of one year and resolution of one hour or better. These data were used in the model but are not shown in detail here for anonymization reasons; instead a summary is provided in Table 2.

Table 1. Statistics of process heat demands. The reference load MW_q is the average thermal demand of the sum of all the furnaces.

Furnace	A1	A2	B1	B2	C1	C2	Total
Peak load [MW/MW_q]	1.28	0.25	0.37	0.19	0.19	0.07	1.93
Mean load [MW/MW_q]	0.62	0.06	0.17	0.07	0.05	0.02	1.00
Mean load (rel. to peak)	49 %	24 %	46 %	39 %	28 %	28 %	52 %
σ [MW/MWq]	0.32	0.04	0.12	0.05	0.05	0.05	0.47
σ (rel. to mean)	51 %	73 %	69 %	64 %	91 %	87 %	47 %

The thermal energy that goes into the furnace at each time-step is modelled as the sum of the LHVs of the fuels $f \in \mathcal{F}$ that are being burned at the time, weighted by a fuel type- and furnace-dependent efficiency parameter η_f^{furn} that accounts for the heat that is lost in the flue gas:

$$q_{t,p}^{furn} = \sum_{f \in \mathcal{F}} \eta_f^{furn} \times LHV_f \times \dot{m}_{t,p}^{f,furn} \tag{3}$$

where $\dot{m}_{t,p}^{f,\text{furn}}$ is the mass flow of each fuel being burned at each time-step. The heat that goes into the product itself is calculated as:

$$q_{\text{pr},t,p}^{\text{furn}} = \eta_{\text{pr}}^{\text{furn}} \times q_{t,p}^{\text{furn}} \tag{4}$$

with the furnace-specific $\eta_{\text{pr}}^{\text{furn}}$ accounting for heat lost via radiation, cooling, etc. Similarly, the energy that can be recovered as high temperature waste heat (defined here as temperatures higher that 150°C) is given by another furnace- and fuel-specific parameter $r_{>150}^{\text{furn}}$:

$$w_{t,p}^{\text{furn}} = \sum_{f \in \mathcal{F}} r_{>150}^{\text{furn}} \times \eta_f^{\text{furn}} \times \text{LHV}_f \times \dot{m}_{t,p}^{f,\text{furn}} \tag{5}$$

The efficiency of each furnace when burning natural gas was inferred from yearly-averaged energy flow data including fuel inputs, product heat, flue gas heat and cooling loads. For simplicity, the efficiencies for other fuels were extrapolated by taking into account the different heating values and stoichiometries but not possible changes in heat transfer dynamics.

Table 2. Parametrization of furnaces in the MILP model.

Furnace	Prod. eff.	Fuel efficiency			Waste heat >150ºC		
	$\eta_{\text{pr}}^{\text{furn}}$	$\eta_{\text{NG}}^{\text{furn}}$	$\eta_{H_2}^{\text{furn}}$	$\eta_{\text{lgSNG}}^{\text{furn}}$	$r_{\text{NG}}^{\text{furn}}$	$r_{H_2}^{\text{furn}}$	$r_{\text{lgSNG}}^{\text{furn}}$
A1	0.660	0.868	0.886	0.869	0.112	0.112	0.112
A2	0.440	0.758	0.773	0.759	0	0	0
B1	0.733	0.833	0.850	0.834	0	0	0
B2	0.500	0.762	0.777	0.763	0	0	0
C1	0.708	0.837	0.854	0.838	0.031	0.031	0.031
C2	0.575	0.870	0.887	0.871	0.029	0.029	0.029

Utilities

In the following the external connections available to the plant are described. These comprise:

Gas grid. Most of the energy demand in the business-as-usual (BAU) case is supplied via natural gas pipeline. Since the gas prices are specific to every mill and usually extremely confidential, in this study a fixed price $c_{\text{buy}}^{\text{NG}}$ = 40 EUR/MWh is used, based on the historical average of 38.97 EUR/MWh (in nominal terms) between 2010 and 2024 [23]. The capacity of the gas pipeline used for supplying the mill is not a relevant constraint, as it covers all the current demand and, in any decarbonization scenario, the use of natural gas is unlikely to increase significantly – quite the opposite.

Biomethane. A small amount of carbon emissions, caused by carbon slip in the CC subsystem, may be offset by purchasing biomethane at a price $c_{\text{buy}}^{\text{BM}}$, which is has an emissions factor ef^{BM} of embedded biogenic carbon. This quantity is approximated as the stochiometric carbon content of the fuel, such that a zero emissions solution is feasible. The capacity of the biomethane delivery system (be it pipeline or trucks) is not considered a significant constraint, as the demand of biomethane allowed in the decarbonized system is considerably lower than the current demand of natural gas. An Austrian government survey of several existing biomethane production sites quotes a production cost between 102 and 182 EUR/MWh [24]. Additionally, a German study on development potential for green gases puts the costs of waste-sourced biomethane at 118 EUR/MWh in the baseline scenario [25]. Thus, in the present model a future price of $c_{\text{buy}}^{\text{BM}}$ = 120 EUR/MWh is assumed.

The OPEX associated with gas and biomethane are:

$$\text{OPEX}^{\text{gas}} = \sum_{p\in\mathcal{P}}\sum_{t\in\mathcal{T}}\left(c_{\text{buy}}^{\text{NG}} \times \dot{m}_{\text{CH}_4,t,p}^{\text{NG}} + c_{\text{buy}}^{\text{BM}} \times \dot{m}_{\text{CH}_4,t,p}^{\text{BM}}\right) \tag{6}$$

Power grid. The power grid is currently the main electricity supply infrastructure. The cost is approximated as a constant $c_{\text{buy}}^{\text{p}}$, with the option to feed-in excess renewable production to the grid at a price $c_{\text{sell}}^{\text{p}}$. The operating costs associated to the power grid are:

$$\text{OPEX}^{\text{power}} = \sum_{p\in\mathcal{P}}\sum_{t\in\mathcal{T}}\left(c_{\text{buy}}^{p} \times p_{t,p}^{\text{buy}} + c_{\text{sell}}^{p} \times p_{t,p}^{\text{sell}}\right) \tag{7}$$

According to data from the International Energy Agency, during the decade and a half from 2010 to 2024 the average spot price for electricity in Austria was 76.47 EUR/MWh in nominal terms [26]. As detailed forecasting of future energy market dynamics falls outside the scope of this work, for the purposes of the MILP model a constant nominal price of $c_{\text{buy}}^{\text{p}}$ = 80 EUR/MWh is used as a proxy for year-round averages. For excess power, the feed-in income is set at $c_{\text{sell}}^{\text{p}}$ = -55 EUR/MWh. This value is set somewhat below the levelized cost of electricity for wind power, so that the grid is allowed to provide some flexibility in times of high generation without the sale of renewable electricity becoming the main business case by itself.

Hydrogen grid. It is expected that in the future it will be possible to import a volume $\dot{m}_{\text{H}_2,t,p}^{\text{buy}}$ of green hydrogen through the existing gas pipeline infrastructure at a price $c_{\text{buy}}^{\text{H}_2}$. The chosen price reflects a midpoint of the 93~171 EUR/MWh projected for pipeline imports into Austria plus some costs for end-user distribution [27], and also takes into account the future production costs targeted by the penalty-and-investment mechanism envisioned in the Austrian ministry's draft Renewable Gases Act [28]. The pipeline in the model also allows to export excess green hydrogen at a rate $m_{\text{H}_2,t,p}^{\text{sell}}$ and price $c_{\text{sell}}^{\text{H}_2}$ when it is not needed on-site. The income is set at a much lower value of 55 EUR/MWh as a deliberate modelling choice to reflect the assumption that feed-in of hydrogen will happen at times of high supply, and thus low market price, across the region. The hydrogen grid-associated OPEX are thus calculated as:

$$\text{OPEX}^{\text{H}_2} = \sum_{p\in\mathcal{P}}\sum_{t\in\mathcal{T}}\left(c_{\text{buy}}^{\text{H}_2} \times \text{LHV}_{\text{H}_2} \times \dot{m}_{\text{H}_2,t,p}^{\text{buy}} + c_{\text{sell}}^{\text{H}_2} \times \text{LHV}_{\text{H}_2} \times \dot{m}_{\text{H}_2,t,p}^{\text{sell}}\right) \tag{8}$$

CO_2 Emissions. For calculation of the business-as-usual (BAU) scenario, the CO_2 emissions certificates need to be taken into account at price $c_{\text{emit}}^{CO_2}$:

$$\mathrm{OPEX}^{\mathrm{CO_2}} = \sum_{p\in\mathcal{P}}\sum_{t\in\mathcal{T}}\left(c_{\mathrm{emit}}^{\mathrm{CO_2}} \times \left(\dot{m}_{\mathrm{CO_2,emit},t,p} - \mathrm{ef}^{\mathrm{BM}} \times \dot{m}_{\mathrm{BM,emit},t,p}\right)\right) \quad (9)$$

As of 2026, the current price of CO_2 emissions certificates in Austria is set by law at 55 EUR/t [29]. However, from 2027 on, the prices will be set dynamically in the EU-wide emissions trading system, with a recent forecast giving a predicted price of 145 EUR/ton by 2030 in the baseline scenario [30]. Thus, as a middle point for the near future, it seems reasonable to set the model's emissions price at $c_{\mathrm{emit}}^{\mathrm{CO_2}}$ = 100 EUR/t.

Table 3. Parametrization of utility prices in the MILP model

Utility	Parameter	Symbol	Value	Reference
Natural gas	Capacity	$\dot{m}_{\mathrm{CH_4,peak}}$	Unlimited	see text
	Price (buy)	$c_{\mathrm{buy}}^{\mathrm{NG}}$	40 EUR/MWh	[23]
Biomethane	Capacity	$\dot{m}_{\mathrm{BM,peak}}$	Unlimited	see text
	Price (buy)	$c_{\mathrm{buy}}^{\mathrm{BM}}$	120 EUR/MWh	[24, 25]
	Emissions factor	$\mathrm{ef}^{\mathrm{BM}}$	2,743 tCO_2/t	see text
Electricity	Capacity	p_{peak}	Varies	scenario-dependent
	Price (draw)	c_{buy}^{p}	80 EUR/MWh	[26]
	Price (feed-in)	c_{sell}^{p}	-55 EUR/MWh	see text
H_2	Capacity	$\dot{m}_{\mathrm{H_2,peak}}$	Unlimited	see text
	Price (draw)	$c_{\mathrm{buy}}^{\mathrm{H_2}}$	150 EUR/MWh	[27, 28]
	Price (feed-in)	$c_{\mathrm{sell}}^{\mathrm{H_2}}$	-60 EUR/MWh	see text
CO_2 emissions	Cost of emissions	$c_{\mathrm{emit}}^{\mathrm{CO_2}}$	100 EUR/tCO_2	Interpolation from [29] and [30]

Wind power. Onshore wind has had a rapid development in Austria in recent years, with an average net yearly increase of 215 MW in installed capacity [31]. There are already operational wind parks in the studied mill's region with more planned, which enabled the use of historical generation profile data (Table 4). In this work, it is assumed that onshore wind will be the main avenue for expansion of low-emission electricity supply, with wind parks located close enough to the factory that they can be connected directly without relying on the already constrained electrical grid. The specific CAPEX are set such that with amortization and interest they yield a levelized cost of electricity (LCoE) of 60 EUR/MWh, in line with the Fraunhofer Institute's 53~68 EUR/MWh estimate of current LCoE for onshore wind in regions with 2500 full load hours [32], which is very close to the 27% average load factor shown in Table 4. If the time-dependent load factor is LF^{wind}, then the supplied electricity is:

$$p_{t,p}^{\mathrm{wind}} = LF_{t,p}^{\mathrm{wind}} \times p_{\mathrm{peak}}^{\mathrm{wind}} \quad (10)$$

Solar PV. As of 2023 Austria had nearly 6.4 GW of solar PV installed capacity, representing a ten-fold increase over the previous decade [33]. In the studied steel mill, a modest surface area was considered suitable for onsite PV installation, potentially acting as a complement to wind power. The generated electricity is proportional to the solar irradiation I^{PV} through the efficiency η^{PV}, and the surface area that can be built is capped at $a_{\mathrm{max}}^{\mathrm{PV}}$:

$$p_{t,p}^{\mathrm{PV}} = I_{t,p}^{\mathrm{PV}} \times \eta^{\mathrm{PV}} \times a^{\mathrm{PV}}, \qquad a^{\mathrm{PV}} \leq a_{\max}^{\mathrm{PV}} \tag{11}$$

For utility-scale PV, the Fraunhofer report cites a CAPEX range of 700~900 EUR/kWp, which amounts to 140~180 EUR/m^2 under 20% efficiency and the standard 1 kW/m^2 [32]. Such value for the efficiency is in the 18~25% range observed for commercial PV modules in another Fraunhofer study [34]. Here a more conservative value of $c_{\mathrm{inv}}^{\mathrm{PV}}$ = 250 EUR/m^2 is used to account for lower irradiance, land acquisition costs, and taxes.

Hydropower. A small capacity of hydropower is currently installed that supplies part of the baseline electrical demand. However it was considered not feasible to expand beyond the current capacity. The load factor is $LF_{t,p}^{\mathrm{hydro}}$, thus:

$$p_{t,p}^{\mathrm{hydro}} = LF_{t,p}^{\mathrm{hydro}} \times p_{\mathrm{peak}}^{\mathrm{hydro}} \tag{12}$$

The investment cost for renewable generation is:

$$\mathrm{CAPEX}^{\mathrm{ren}} = c_{\mathrm{inv}}^{\mathrm{wind}} \times p_{\mathrm{peak}}^{\mathrm{wind}} + c_{\mathrm{inv}}^{\mathrm{PV}} \times a^{\mathrm{PV}} \tag{13}$$

Table 4. Statistics of renewable generation profiles.

Technology	Parameter	Symbol	Peak	Mean	σ	H when =0
Wind	Load factor	$LF_{t,p}^{\mathrm{wind}}$	1.00	0.27	0.30	15 %
Solar PV	Irradiance	$I_{t,p}^{\mathrm{PV}}$	886 W/m^2	133 W/m^2	213 W/m^2	47 %
Hydro	Load factor	$LF_{t,p}^{\mathrm{hydro}}$	1.00	0.44	0.23	0 %

Table 5. Parametrization of renewable energy sources in the MILP model.

Technology	Parameter	Symbol	Value	Reference
Wind	Specific CAPEX	$c_{\mathrm{inv}}^{\mathrm{wind}}$	3,614 kEUR/MW	60 EUR/MWh [32]
PV	Efficiency	η^{PV}	20 %	[34]
	Maximum area	$a_{\max}^{\mathrm{PV}}$	717 m^2/MW$_{\mathrm{q}}$	Site measurements
	Specific CAPEX	$c_{\mathrm{inv}}^{\mathrm{PV}}$	250 EUR/m^2	Computed from [32]

Electrolysis Subsystem

Green hydrogen is produced by electrolysis of purified water using green electricity, either directly from renewable power or with power drawn from the electrical grid with the appropriate green generation certificates. In some cases, a heat input is also required to maintain the temperature of the reaction.

In general, the electrolyser stack is modelled as a linear relation between the power input $p_{t,p}^{\mathrm{elec}}$ and heat input $q_{t,p}^{\mathrm{elec}}$ on one side and the mass flow output of hydrogen $\dot{m}_{\mathrm{H_2},t,p}^{\mathrm{elec}}$ on the other:

$$\dot{m}_{\mathrm{H_2},t,p}^{\mathrm{elec}} = \frac{\eta^{\mathrm{elec}}}{\mathrm{LHV}_{\mathrm{H_2}}} \times \left(p_{t,p}^{\mathrm{elec}} + q_{t,p}^{\mathrm{elec}}\right) \tag{14}$$

where η^{elec} is the efficiency of the electrolyser stack and LHV_{H_2}=119.96 MJ/kg is the lower heating value of hydrogen. For the capacity-expansion model used in this work, AWE/PEM and SOEC units are represented with constant efficiency over their admissible operating range. This simplification is consistent with the planning focus of the model, which prioritizes long-term investment, sizing, and infrastructure interactions over detailed stack electrochemistry. This simplified model improves the computational tractability at the cost of slightly overestimating efficiency at low part load.

There is a maximum fraction $rq_{\max}^{elec}$ of energy that can be supplied directly as heat:

$$q_{t,p}^{elec} \leq rq_{\max}^{elec} \times \left(p_{t,p}^{elec} + q_{t,p}^{elec}\right) \tag{15}$$

and also a technology-dependent minimal part load, such that if the nominal capacity is $m_{H_2,peak}^{elec}$ and the minimal load is $\lim_{min}^{elec}$, then depending on whether the electrolyser is active:

$$\dot{m}_{H_2,t,p}^{elec} \begin{cases} \in \left[\lim_{min}^{elec} \times \dot{m}_{H_2,peak}^{elec}, \dot{m}_{H_2,peak}^{elec}\right], & \text{if electrolyser is running} \\ = 0, & \text{if electrolyser is shut down} \end{cases} \tag{16}$$

The logic of (16) is implemented in the MILP framework by using a binary time series commitment variable paired with the appropriate constraints.

Alkaline Water Electrolysis (AWE) and Proton Electron Membrane electrolysis (PEM). In AWE, OH^- anions move from cathode to anode through a liquid electrolyte, releasing H_2 gas at the cathode. In PEM, water is supplied at the anode and H+ cations traverse a polymer membrane to the cathode, forming H_2 gas at the cathode. While both types of electrolysis have their own specificities, in the linearized approach of this work they are grouped together due to their generally lower investment cost, lower efficiency, room-temperature operation and lower minimal part load, the latter being relevant when dealing with intermittent renewable energy sources [35]. The investment cost of $c_{inv}^{AWE/PEM}$ = 850 kEUR/MW was quoted by an industry insider source, but it lines up with the upper band of the forecasted range laid out at the beginning of the decade by the Fraunhofer institute, which is a system cost of 450~950 kEUR/MW for AWE and 500~980 kEUR/MW for PEM, with the upper limit corresponding to 5 MW-scale in 2020 and the lower one for 100 MW-scale in 2030 [36]. The constant part load efficiency of 62%, assumed for both technologies (Eq. 14) in line with a 52.8~55.1 kWh/kg system electricity demand [36], is valid for PEM electrolysers in the range of around 40% to 100% load. Below 40% a drop in efficiency can be expected.

Solid Oxide Electrolysis Cell (SOEC). In SOEC, high-temperature steam is supplied at the cathode and O^{2-} anions are transported from cathode to anode through a solid ceramic membrane. This type of technology has a higher investment cost, higher efficiency, heat for steam generation as part of the energy input (which can be supplied as waste heat from other processes) and a more restrictive minimal part load, which complicates its use with intermittent renewable sources [35]. The investment costs of c_{inv}^{SOEC} = 3,750 kEUR/MW were provided by industry insider sources, including not just the electrolysis cells but also heat integration and the associated infrastructure. This lines up reasonably with costs reported in the literature – the World Bank reported 5,000~5,800 kUSD/MW for current pilot projects and a potential for cost reduction to 2,000 kUSD/MW in upscaled systems [37], while another report in the European context projected 4,800 kEUR/MW in the base case for 2020 and 1,200 EUR/MW for the upscaled system in 2030 [38].

If $\dot{m}_{\mathrm{H_2,peak}}^{\mathrm{AWE/PEM}}$ and $\dot{m}_{\mathrm{H_2,peak}}^{\mathrm{SOEC}}$ are the nominal capacities selected for the respective technologies, then the investment costs for the electrolysis subsystem are:

$$\mathrm{CAPEX}^{\mathrm{elec}} = c_{\mathrm{inv}}^{\mathrm{AWE/PEM}} \times \mathrm{LHV}_{\mathrm{H_2}} \times \dot{m}_{\mathrm{H_2,peak}}^{\mathrm{AWE/PEM}} + c_{\mathrm{inv}}^{\mathrm{SOEC}} \times \mathrm{LHV}_{\mathrm{H_2}} \times \dot{m}_{\mathrm{H_2,peak}}^{\mathrm{SOEC}} \quad (17)$$

Table 6. Parametrization of electrolysis technologies in the MILP model.

Technology	Parameter	Symbol	Value	Reference
AWE/PEM	Efficiency	$\eta^{\mathrm{AWE/PEM}}$	62 %	Calculated from [36]
	Minimal load	$\mathrm{lim}_{\mathrm{min}}^{\mathrm{AWE/PEM}}$	5 %	[39]
	Maximal heat ratio	$rq_{\mathrm{max}}^{AWE/PEM}$	0 %	[39]
	Specific CAPEX	$c_{\mathrm{inv}}^{\mathrm{AWE/PEM}}$	850 kEUR/MW	Industry source, supported by [36]
SOEC	Efficiency	η^{SOEC}	75 %	[40]
	Minimal load	$\mathrm{lim}_{\mathrm{min}}^{\mathrm{SOEC}}$	50 %	[40]
	Maximal heat ratio	$rq_{\mathrm{max}}^{\mathrm{SOEC}}$	20 %	[40]
	Specific CAPEX	$c_{\mathrm{inv}}^{\mathrm{SOEC}}$	3,750 kEUR/MW	Industry source, supported by [37, 38]

Carbon Capture Subsystem

In the reheating furnace context, post-combustion carbon capture consists generally of collecting the flue gas of furnaces and passing it through a device that separates the CO_2 from the rest of the flue gas, so that it can be either stored away or utilized in some other process. In this case, the purpose of the CC is to produce SNG that is burned again in the furnaces, in a quasi-closed loop. The carbon capture process requires electricity and/or heat to separate the CO_2 from the rest of the species in the flue gas, with the specific values varying by technology. Assuming constant efficiency over the operating range, the linearised input-output relations for a CC unit with recovery rate R^{CC}, power demand d_p^{CC} and heat demand d_q^{CC} are:

$$\dot{m}_{\mathrm{CO_2,cap},t,p}^{\mathrm{CC}} = R^{\mathrm{CC}} \times \dot{m}_{\mathrm{CO_2,in},t,p}^{\mathrm{CC}}, \qquad \dot{m}_{\mathrm{CO_2,slip},t,p}^{\mathrm{CC}} = (1-R) \times \dot{m}_{\mathrm{CO_2,in},t,p}^{\mathrm{CC}} \quad (18)$$

$$p_{t,p}^{\mathrm{CC}} = d_p^{\mathrm{CC}} \times \dot{m}_{\mathrm{CO_2,in},t,p}^{\mathrm{CC}}, \qquad q_{t,p}^{\mathrm{CC}} = d_q^{\mathrm{CC}} \times \dot{m}_{\mathrm{CO_2,in},t,p}^{\mathrm{CC}} \quad (19)$$

where the subindices "in", "cap" and "slip" refer to the mass flows of CO_2 that comes in with the flue gas, that is captured, and that slips from the CC unit without being captured, respectively.

A multitude of different CC technologies exist, divided into several families and at different technology readiness levels (TRL) [41]. In this work, two possibilities from the absorption family and one from the adsorption family are considered.

Amine Scrubber (AS). This method works by passing the flue gas through an amine bath in a continuous process. The amine is then regenerated and the CO_2 stored. The process has a low power demand but higher heat requirements, and is currently at a very high TRL [41]. The investment costs are taken to be $c_{\mathrm{inv}}^{\mathrm{AS}} = 225$ kEUR/(t/h), based on quotes from suppliers.

Amine Scrubber with Heat Pump (ASHP). The AS process can be made more efficient by integrating a heat pump for internal heat recovery. This eliminates the need for external heat

input and replaces it with a smaller electricity input, at the cost of higher installation costs [42]. Those costs $c_{\text{inv}}^{\text{ASHP}} = 1.697$ kEUR/(t/h) are based on the costs for the AS itself plus the cost premium for the heat pump provided in the aforementioned paper.

Pressure Swing Adsorption (PSA). This method separates CO_2 by feeding flue gas into a pressurized tank and then greatly reducing the pressure of the tank, which causes the CO_2 to be adsorbed into a purposefully designed solid coating (typically zeolite-based) while the other components of the gas remain free. This batch process requires no heat input but instead is powered by electricity, and although its TRL for CO_2 capture is lower, it is considered in the literature to promise low operation and investment costs [41, 43]. As exact costs figures for this type of system are hard to find in the literature, an estimate of $c_{\text{inv}}^{\text{PSA}} = 1{,}111$ kEUR/(t/h) has been calculated from two studies that provide partial cost figures [44, 45].

As the CC units should ideally be located as close as possible to the source of the flue gas, the system is envisioned as two separate parts: a choice of AS, ASHP and/or PSA for the group of furnaces A/B and another for the pair of furnaces C, with access to recovered waste heat shared between all. This is illustrated on the right side of Figure 1. If the nominal capacity of each unit in terms of captured mass per unit of time is $\dot{m}_{\text{CO}_2,\text{peak}}^{\text{CC}}$, then the associated investment costs are:

$$\begin{aligned}\text{CAPEX}^{\text{CC}} = c_{\text{inv}}^{\text{AS}} \times \left(\dot{m}_{\text{CO}_2,\text{peak}}^{\text{AS,A/B}} + \dot{m}_{\text{CO}_2,\text{peak}}^{\text{AS,C}}\right) + c_{\text{inv}}^{\text{ASHP}} \times \left(\dot{m}_{\text{CO}_2,\text{peak}}^{\text{ASHP,A/B}} + \dot{m}_{\text{CO}_2,\text{peak}}^{\text{ASHP,C}}\right) \\ + c_{\text{inv}}^{\text{PSA}} \times \left(\dot{m}_{\text{CO}_2,\text{peak}}^{\text{PSA,A/B}} + \dot{m}_{\text{CO}_2,\text{peak}}^{\text{PSA,C}}\right)\end{aligned} \quad (20)$$

Table 7. Parametrization of carbon capture technologies in the MILP model.

Technology	Parameter	Symbol	Value	Reference
AS	Separation rate	R^{AS}	95.0 %	[46]
	Heat demand	d_q^{AS}	3.79 MJ/kg	[46]
	Electricity demand	d_p^{AS}	0.1744 MJ/kg	[46]
	Specific CAPEX	$c_{\text{inv}}^{\text{AS}}$	225 kEUR/(t/h)	Industry sources
ASHP	Separation rate	R^{ASHP}	95.0 %	[42]
	Heat demand	d_q^{ASHP}	-	[42]
	Electricity demand	d_p^{ASHP}	1.62 MJ/kg	[42]
	Specific CAPEX	$c_{\text{inv}}^{\text{ASHP}}$	1.697 kEUR/(t/h)	[42]
PSA	Separation rate	R^{PSA}	98.2 %	[43]
	Heat demand	d_q^{PSA}	-	[43]
	Electricity demand	d_p^{PSA}	1.7 MJ/kg	[43]
	Specific CAPEX	$c_{\text{inv}}^{\text{PSA}}$	1,111 kEUR/(t/h)	Estimate from [44] and [45]

Synthetic Natural Gas Subsystem

Hydrogen (H_2) and carbon dioxide (CO_2) can react exothermically to produce methane (CH_4). In the ideal reaction, the so-called Sabatier process can be summarised [47] in the following stoichiometric formula:

$$\text{CO}_2 + 4\text{H}_2 \rightarrow \text{CH}_4 + 2\text{H}_2\text{O} + 164.0\ \text{kJ/mol} \quad (21)$$

In a methanation reactor, this reaction can be carried out in a controlled manner to achieve specific compositions and conversion rates, depending on the desired properties of the resulting gas mixture. The fraction of residual carbon dioxide and hydrogen left in the resulting gas depend on the actual stochiometric ratios in the initial mixture and on the respective conversion rates $\chi_{\mathrm{CO_2}}^{\mathrm{meth}}$ and $\chi_{\mathrm{H_2}}^{\mathrm{meth}}$. In the linearized model it is assumed that the reactor is operated at a fixed stochiometric ratio of feedstocks and thus at fixed conversion ratios and waste heat generation Then the linearized input-output relations for the reactor model, relating the CO_2 and H_2 inputs to the CH_4, waste heat, CO_2 and H_2 outputs are, respectively:

$$\dot{m}_{\mathrm{CH_4,out},t,p}^{\mathrm{meth}}=\chi_{\mathrm{CO_2}}^{\mathrm{meth}} \times \dot{m}_{\mathrm{CO_2,in},t,p}^{\mathrm{meth}}, \quad wh_{t,p}^{\mathrm{meth}}=10.2\ \mathrm{MW/(kg/s)} \times \dot{m}_{\mathrm{CH_4,out},t,p}^{\mathrm{meth}} \tag{22}$$

$$\dot{m}_{\mathrm{CO_2,out},t,p}^{\mathrm{meth}}=\left(1-\chi_{CO_2}^{\mathrm{meth}}\right) \times \dot{m}_{\mathrm{CO_2,in},t,p}^{\mathrm{meth}}, \quad \dot{m}_{\mathrm{H_2,out},t,p}^{\mathrm{meth}}=\left(1-\chi_{\mathrm{H_2}}^{\mathrm{meth}}\right) \times \dot{m}_{\mathrm{H_2,in},t,p}^{\mathrm{meth}} \tag{23}$$

One-Stage Methanation (OSM). In a conventional methanation reactor, not all the CO_2 is converted into methane; in addition to a large concentration of CH_4, also some amount of residual H_2 and CO_2 are present. This changes the LHV and flame properties of the fuel with respect to the near-pure methane of natural gas; consequently in this work said mixture is referred to as low-grade synthetic natural gas (lgSNG). All the parameters for this type of reactor were collected from an industry supplier source.

Two-Stage Methanation (TSM). By cooling the lgSNG and passing it through another methanation reactor, a much higher purity of methane can be achieved, making it effectively identical to fossil-sourced natural gas, i.e. [48]. All the parameters for this type of reactor were collected from an industry supplier source as well.

The investment costs associated with the methanation reactor(s) are:

$$\mathrm{CAPEX}^{\mathrm{meth}} = c_{\mathrm{inv}}^{\mathrm{OSM}} \times \dot{m}_{\mathrm{lgSNG,peak}}^{\mathrm{OSM}} + c_{\mathrm{inv}}^{\mathrm{TSM}} \times \dot{m}_{\mathrm{CH_4,peak}}^{\mathrm{OSM}} \tag{24}$$

Table 8. Parametrization of methanation technologies in the MILP model.

Technology	Parameter	Symbol	Value	Reference
OSM	CO_2 conversion rate	$\chi_{\mathrm{CO_2}}^{\mathrm{OSM}}$	94 %	Industry source
	H_2 conversion rate	$\chi_{\mathrm{H_2}}^{\mathrm{OSM}}$	93 %	Industry source
	LHV of SNG	LHV_{lgSNG}	44.52 MJ/kg	Calculated from industry source
	Specific CAPEX	$c_{\mathrm{inv}}^{\mathrm{OSM}}$	820 kEUR/MW	Industry source
TSM	CO_2 conversion rate	$\chi_{\mathrm{CO_2}}^{\mathrm{TSM}}$	100 %	Industry source
	H_2 conversion rate	$\chi_{\mathrm{H_2}}^{\mathrm{TSM}}$	99 %	Industry source
	LHV of SNG	LHV_{SNG}	50.36 MJ/kg	Calculated from industry source
	Specific CAPEX	$c_{\mathrm{inv}}^{\mathrm{TSM}}$	1,172 kEUR/MW	Industry source

Energy Storage

In case of load and or/cost variations in the energy supply (due to the intermittency of renewable sources) or in the energy demand (due to production requirements), energy storage can provide flexibility by smoothing out those fluctuations. In this work two possibilities have been considered: electro-chemical storage in batteries and chemical storage in H_2 tanks. Both are modelled using a linearized approach with a charging/discharging efficiency parameter η and a standing state-of-charge loss λ.

If each storage has a maximum state-of-charge (SoC) capacity $\mathrm{SoC}_{\mathrm{peak}}$, the investment cost for storages is:

$$\mathrm{CAPEX}^{\mathrm{storage}} = c_{\mathrm{inv}}^{\mathrm{bat}} \times \mathrm{SoC}_{\mathrm{peak}}^{\mathrm{bat}} + c_{\mathrm{inv}}^{\mathrm{H_2\ tank}} \times \mathrm{SoC}_{\mathrm{peak}}^{\mathrm{H_2\ tank}} \tag{25}$$

Charging/discharging losses for the battery storage were (somewhat optimistically) considered negligible for the purposes of this study, but auxiliary losses were accounted for at 1%/h as a typical value for multi-MWh-scale, fast-cycling storages [49]. The investment cost was set at $c_{\mathrm{inv}}^{\mathrm{bat}}$=100 kEUR/MWh, in line with European Commission expectations of battery packs falling below 100 USD/kWh in 2027 [50]. For the hydrogen tank storage the round-trip efficiency was set at 80% as an intermediate point between the 60~70% range of liquefied storage and the (pressure-dependent) 80~95% range of compressed storage [51], the auxiliary demand equal to the battery, and the investment cost assumed to be a higher $c_{\mathrm{inv}}^{\mathrm{H_2\ tank}}$ = 400 kEUR/MWh, with these less optimistic parametrization likely favoring batteries.

Table 9. Parametrization of energy storage technologies in the MILP model.

Technology	Parameter	Symbol	Value	Reference
Battery	SoC loss	λ^{bat}	1 %/h	[49]
	Roundtrip eff.	η^{bat}	100 %	Simplification
	Specific CAPEX	$c_{\mathrm{inv}}^{\mathrm{bat}}$	100 kEUR/MWh	[50]
H_2 tank	SoC loss	$\lambda^{H_2\ \mathrm{tank}}$	1 %/h	[49]
	Roundtrip eff.	$\eta^{H_2\ \mathrm{tank}}$	80 %	[51]
	Specific CAPEX	$c_{\mathrm{inv}}^{\mathrm{H_2\ tank}}$	400 kEUR/MWh	Assumption

Objective function

Bringing together eqs. (6), (7), (8) and (9) yields the total annual OPEX:

$$\mathrm{OPEX} = \mathrm{OPEX}^{\mathrm{gas}} + \mathrm{OPEX}^{\mathrm{power}} + \mathrm{OPEX}^{\mathrm{H_2}} + \mathrm{OPEX}^{\mathrm{CO_2}} \tag{26}$$

while the total CAPEX are obtained from eqs. (13), (17), (20), (24) and (25):

$$\mathrm{CAPEX} = \mathrm{CAPEX}^{\mathrm{ren}} + \mathrm{CAPEX}^{\mathrm{elec}} + \mathrm{CAPEX}^{\mathrm{CC}} + \mathrm{CAPEX}^{\mathrm{meth}} + \mathrm{CAPEX}^{\mathrm{storage}} \tag{27}$$

bringing the total annualized costs to:

$$\text{annual cost} = \mathrm{OPEX} + \frac{i(1+i)^n}{(1+i)^n - 1}\mathrm{CAPEX} \tag{28}$$

with an interest rate i =3% and amortization period n =20 years yielding a CAPEX annualization factor of 6.7%.

Scenario definition

It is expected that the grid will be strained in the future due to increased demand both in the plant and in the broader region as both the steel industry and other sectors electrify their processes. Although quantitative forecasts of future grid availability are outside the scope of this work, it was deemed relevant to establish three exploratory scenarios regarding the grid connection regime. The three scenarios respectively represent optimistic, baseline and pessimistic possibilities for the medium-term development of the power grid in the region and in Austria at large.

Unconstrained grid regime. With a peak capacity of around 7.2 MW/MW_q, it represents a scenario where all the investments in grid capacity are realized and the mill can draw, in practice, as much power as it needs from the grid. This boundary condition potentially tilts the optimal solution towards a more interconnected system.

Partially constrained grid regime. With a 0.72 MW/MW_q peak capacity, this roughly corresponds to the current situation before decarbonization and electrification measures are undertaken.

Strongly constrained grid regime. With only 0.24 MW/MW_q of peak capacity available, which equals around one-third of today's maximum theoretical capacity, it represents a pessimistic scenario in which grid expansion investments to alleviate structural bottlenecks lag behind industry decarbonization commitments and thus place limits on the mill's ability to draw electrical power from the grid, potentially pushing the optimal solution towards more electricity-efficient technologies and/or a more self-contained system with expanded onsite renewable generation.

RESULTS AND DISCUSSION

This section consists of three parts. First, the energy costs for both decarbonization routes are studied, as well as the associated optimal design of the energy system. Secondly, a more detailed look is given at the optimal operation of the electrolysis and CC subsystems. Thirdly, a parameter variation analysis is conducted to identify the influence of some of the major model parameters.

Energy costs and optimal design

Figure 2 shows a breakdown of the levelized costs of heat (LCoH), in terms of EUR/MWh of product heat. The most apparent result is that in all scenarios, switching to a decarbonized energy system incurs a stark increase in the LCoH. If hydrogen can be burned directly in the furnaces, the LCoH is shown to increase by between 124% (if the electrical grid is unconstrained) and 166% (if it is strongly constrained). If the CC+SNG subsystem is required, the costs increase further: by 187% in the unconstrained grid (28% more expensive than only hydrogen) and by 231% in the strongly constrained grid (24% more expensive), a more than three-fold increase. There are two main factors for this difference: on the one hand, the additional CAPEX and OPEX associated with the CC+SNG subsystem, which are not present in the pure-H_2 path; on the other, the additional CAPEX and OPEX induced in the electricity and hydrogen supplies, due to the conversion losses in the methanation step and to the lower combustion efficiency of SNG relative to hydrogen. The results are consistent with the lower end of the 25~43% bracket that Zabik, Birkelbach et al. found for the SNG cost premium [17].

Upon a closer look at the individual grid scenarios, some interesting differences arise, which can be explained by the Sankey diagrams of energy flows in Figs. Figure 3 and Figure 4:

Unconstrained grid. In the unconstrained grid scenario (top bar of each trio in Figure 2), most of the electricity is supplied directly from the grid, with only a minor contribution from wind power, and lesser amounts from hydro and PV, with no battery storage required. Hydrogen is produced largely onsite with a smaller contribution from grid purchases.

Partially constrained grid. In the partially constrained grid scenario (middle bar), around half of the electricity demand is satisfied by the grid and the other half by renewables (mostly wind) and some battery storage. However, the total electricity consumption is low, because the optimal solution involves purchasing most hydrogen from the grid.

Strongly constrained grid. In the scenario where the grid is most strongly constrained (bottom bar), it can only supply part of the necessary electrical power, so a large capacity of wind power is installed and there is also substantial buying of hydrogen from the grid. Flexibility to offset the intermittency of wind generation is provided through three mechanisms: exporting excess electricity to the grid, charging or discharging the battery storage depending on the supply and demand at each time step, and producing excess hydrogen and exporting it.

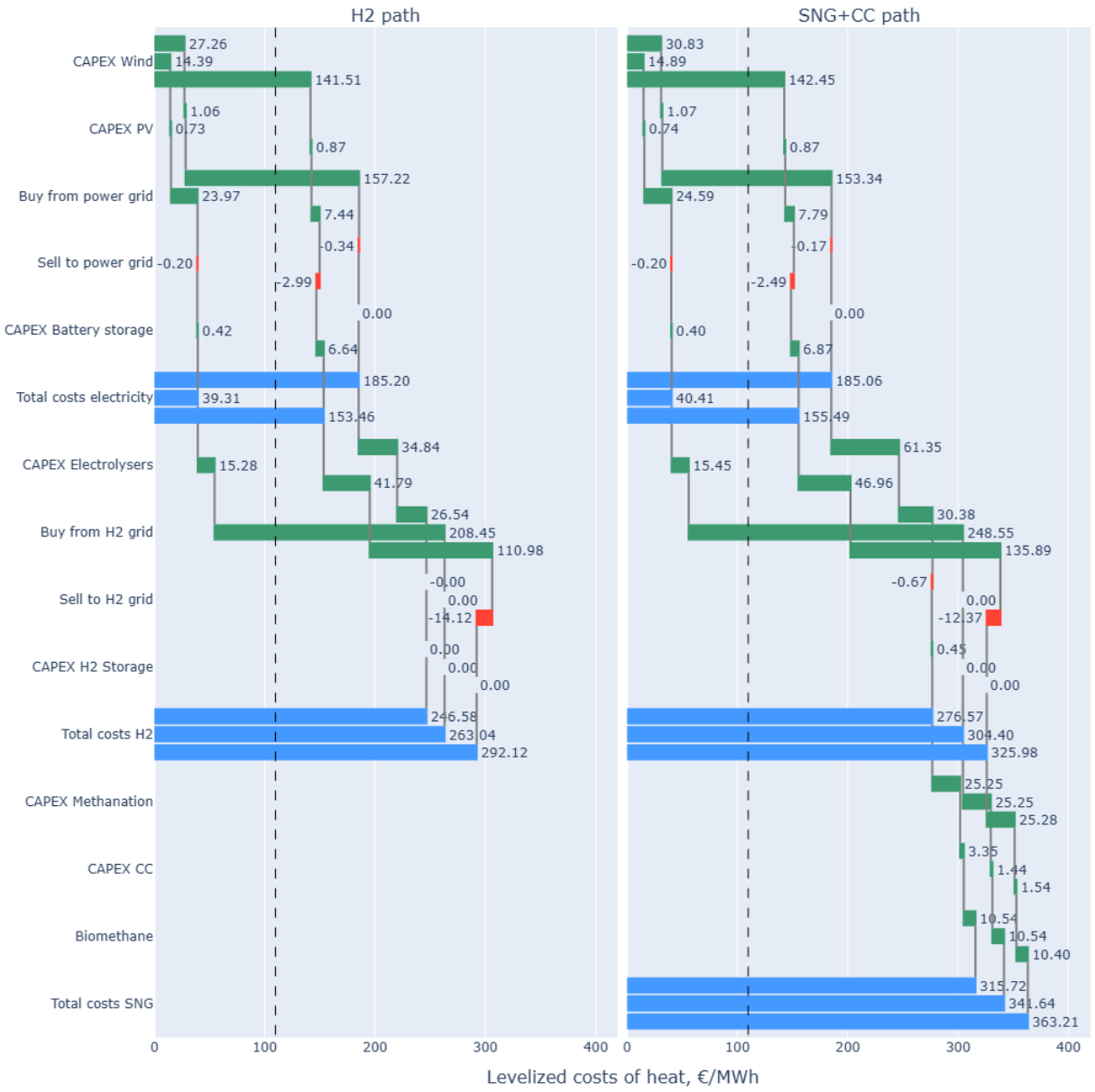

Figure 2. Waterfall plot for the cost breakdown in both the H2 and the SNG path, including expenses (green), incomes (red) and intermediate totals (blue). For each trio of bars, the top series is for the unconstrained grid case; the middle one, for the partially constrained grid; and the one in the bottom, for the strongly constrained grid. The dashed line marks the BAU case cost of 109.80 EUR/MWh, consisting of 73.80 EUR/MWh of natural gas costs and 36.00 EUR/MWh of emissions certificates.

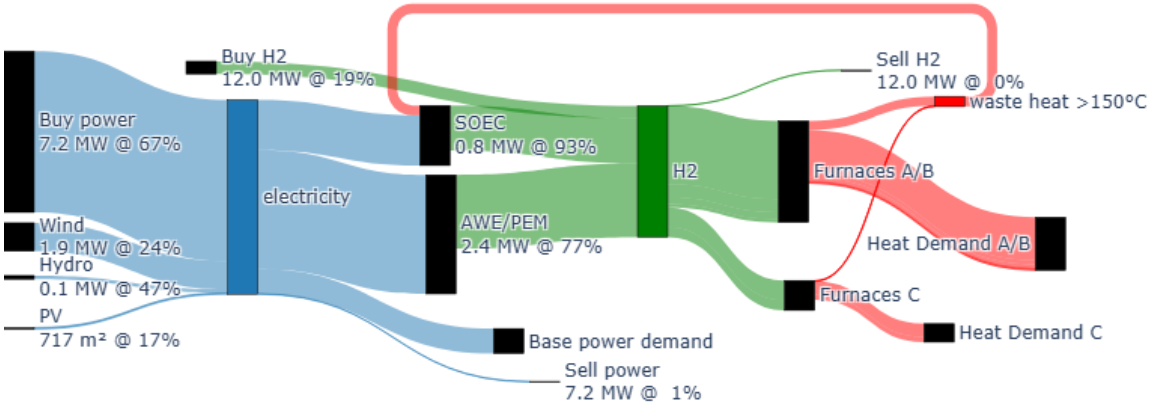

(a)

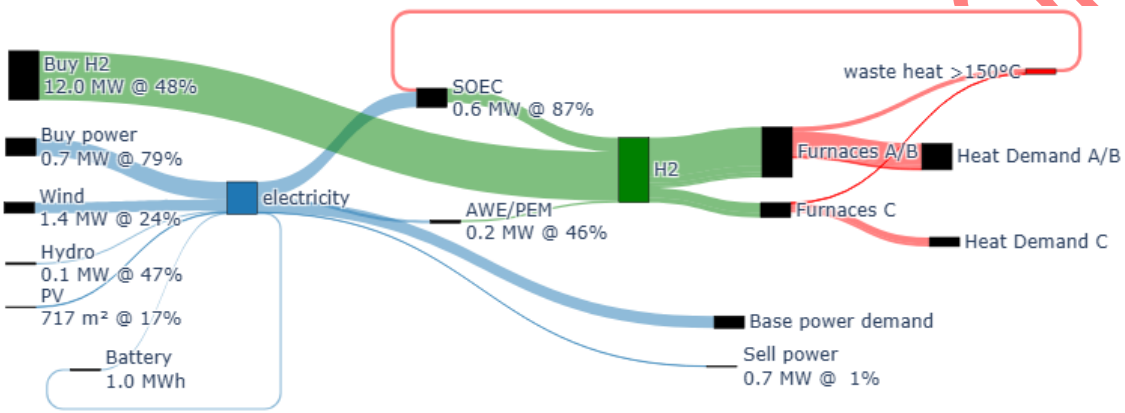

(b)

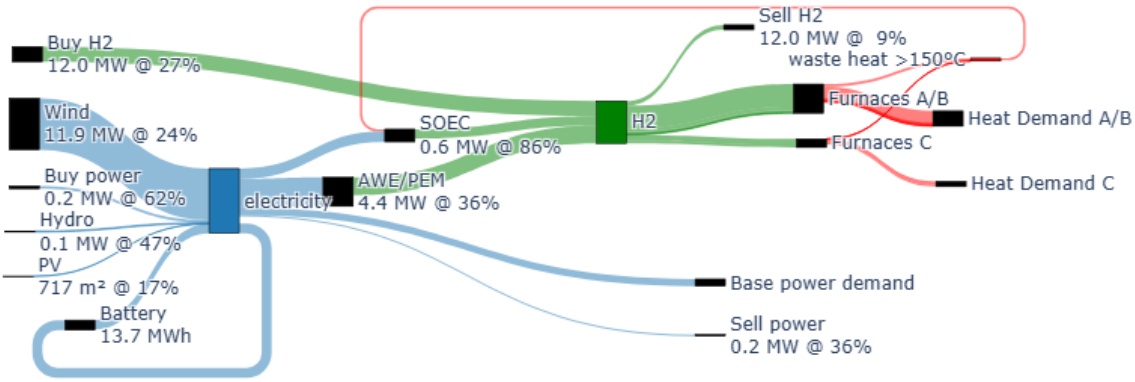

(c)

Figure 3. Sankey diagrams of the optimal systems for the H_2 route (a: unconstrained grid; b: partially constrained grid; c: strongly constrained grid). All quantities are peak capacities per MW of product heat; the quoted percentages are each unit's average load factor. The diagrams are not to scale with each other; the heat demand is the same in all cases.

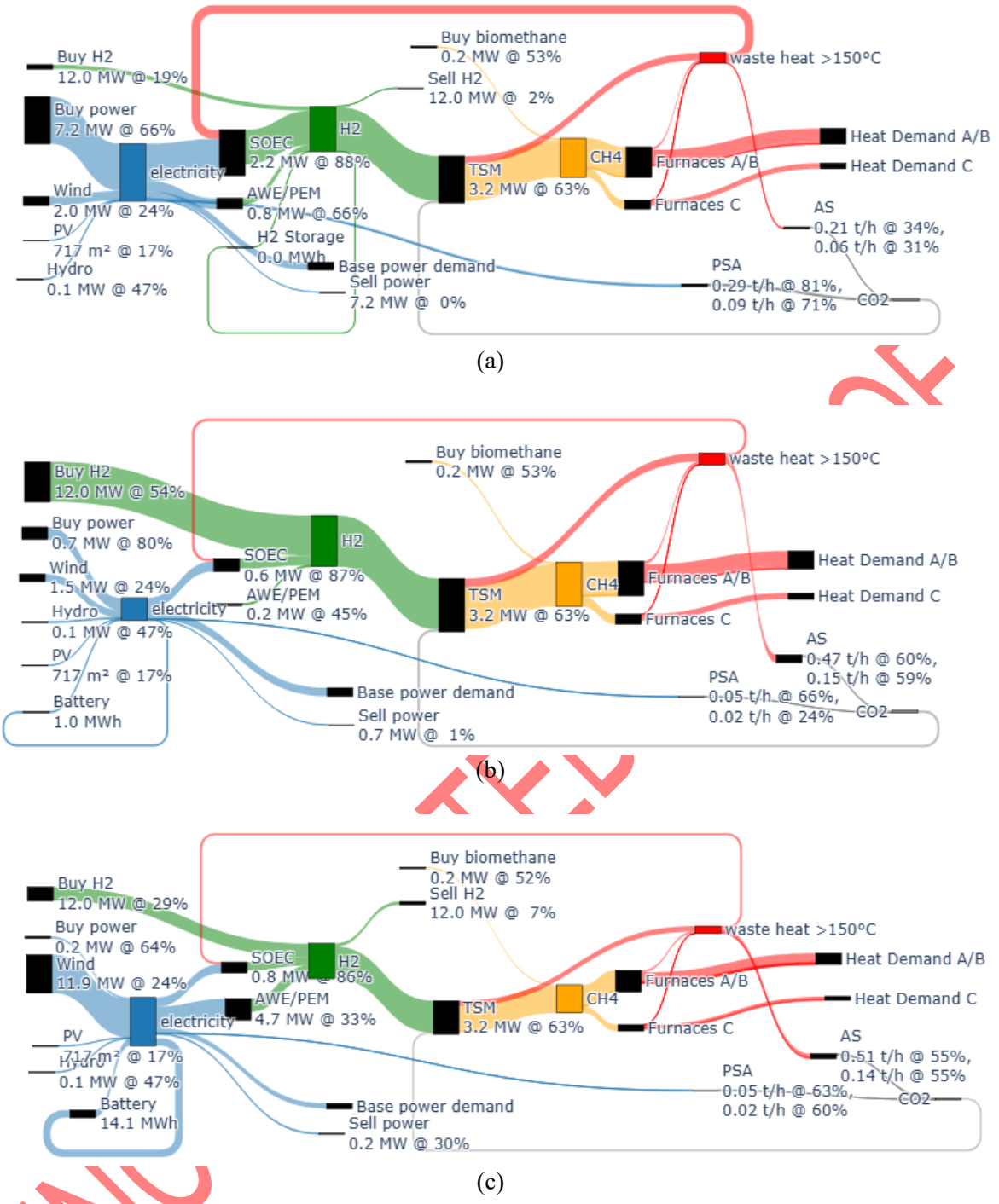

Figure 4. Sankey diagrams of the optimal systems for the CC+SNG route (top: unconstrained grid; middle: partially constrained grid; bottom: strongly constrained grid). All quantities are peak capacities per MW of product heat; the quoted percentages are each unit 's average load factor. CO_2 slip and emissions compensation from biomethane are not shown. In the CC units, the upper row is for A/B and the lower row for C.

CAPEX-OPEX trade-offs and optimal operation

When different options are available whose OPEX and CAPEX form a Pareto front, optimization can show which of them, or which combination of them, offers the lowest total cost under a set of boundary conditions. The optimal operating patterns optimized

simultaneously with the capacity decisions shown in Figure 3 and Figure 4 are highlighted in the following.

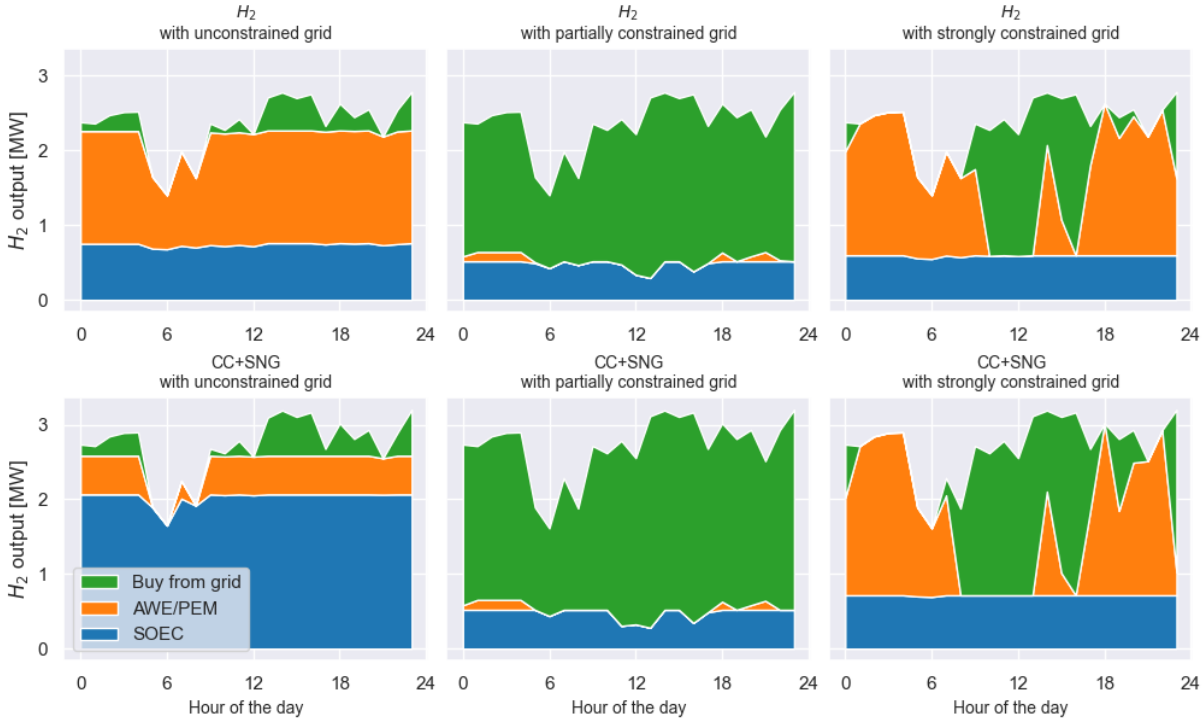

Figure 5. Optimal operation of the electrolysis subsystem for both routes and under the three grid scenarios, during one of the representative days.

Electrolysis subsystem. Figure 5 shows the operation of the electrolysis subsystem during one of the 24-hour representative periods (specifically, October 10th). It is apparent from the plots that, regardless of the decarbonization route and grid capacity the three methods of supplying green H_2 fulfil specific roles. First, the high-CAPEX, low-OPEX SOEC acts as a base load supply, operating at a near-constant, very high load factor which takes advantage of its high efficiency to offset the larger investment cost. Second, the low-CAPEX, high-OPEX AWE/PEM follows the demand profile more closely whenever abundant wind power is available (typically at night), taking advantage of its more flexible operation possibilities. Finally, the option to directly purchase green hydrogen from the grid is used for peak-of-the-peak supply, thus avoiding extra electrolyser capacity that would otherwise go largely unused; it is also used to fulfil variable loads when the availability of wind power is low, particularly in the partially constrained grid scenario.

Looking more closely at the three grid scenarios, some extra insights can be gained. When the grid is unconstrained, the electrolyser capacity is dominated by AWE/PEM in the H_2 route and by SOEC in the CC+SNG route. This is due to the highly exothermal nature of the methanation process increasing the availability of waste heat, which can be reused in the SOEC unit to further lower its operational costs. Meanwhile, in the strongly constrained scenario, the intermittency of renewable generation causes the AWE/PEM to dominate the optimal solution - a higher capacity of SOEC would require a higher base load supply of electricity, in turn necessitating additional investment in battery storage. The role of storage is in any case quite limited, in line with the static price scenarios from Zabik, Birkelbach et al., and would presumably be more relevant if fluctuating prices were introduced into the model [17].

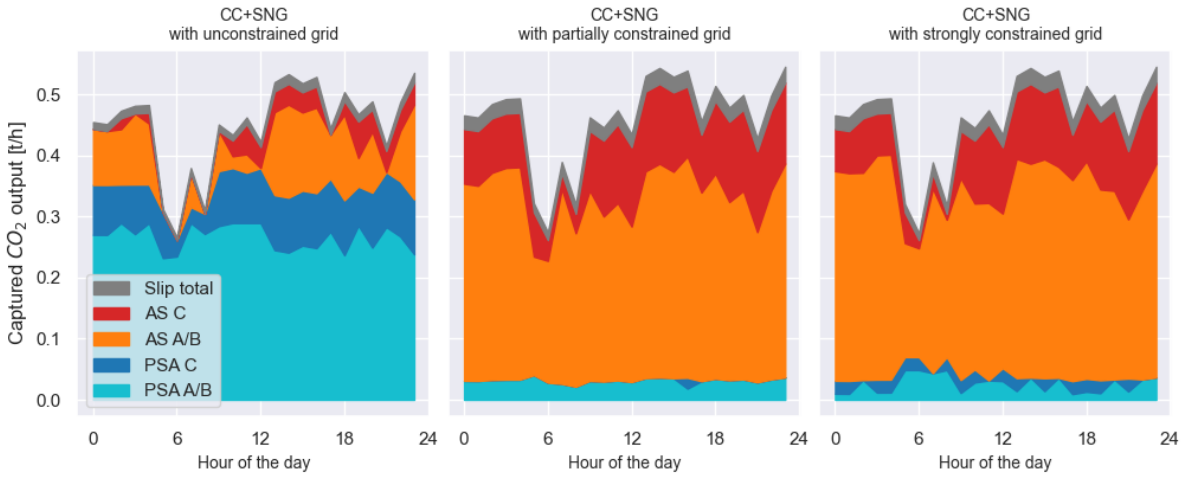

Figure 6. Optimal operation of the carbon capture subsystem under the three grid scenarios, during the same representative day.

CC subsystem. In the carbon capture subsystem, meanwhile, the optimal operation is strongly related with the availability of electricity. In the unconstrained grid scenario, the PSA (using abundant electricity) is used to fulfil the baseline demand, while the AS (using waste heat for which it competes with the SOEC) is activated as a backup when the load of the furnaces is high. In the two constrained grid scenarios, on the other hand, the PSA provides a small, uniform capacity while the AS handles most of the carbon capture demand. In these two latter scenarios, due to the lower capture rate, a larger carbon slip is present which must be offset by a larger purchase of biomethane. These results again highlight the crucial role that the grid conditions have on the optimal decarbonization strategy.

In scenarios with unconstrained grid access, the model favours technologies with higher investment cost but lower operating cost and/or higher efficiency, because sufficient electricity is available to utilize them at high load factors. This leads to steadier operation of units such as SOEC and PSA. By contrast, under constrained grid conditions the model shifts toward more flexible technologies and supply options, including AWE/PEM, hydrogen imports, wind power and storage, because electricity scarcity increases the value of operational flexibility. Thus, the optimal design and the optimal operation should be interpreted jointly: the installed capacities reflect the expected operating regime, while the operating profiles explain why those capacities are economically preferred.

Parameter variations

It follows from Figure 2 that the CAPEX of wind power, the cost of purchasing green hydrogen from the gas grid and the CAPEX of the electrolysers are some of the largest contributors to the total energy costs. However, there is considerable uncertainty in the values of those parameters, which may cause significant deviations in the actual energy costs. Therefore, a sensitivity analysis was conducted to study if and to what extent the possible changes in those parameters affect the LCoH.

Wind CAPEX. The 60 EUR/MWh LCoE assumed for the onshore wind production is realistic but somewhat on the optimistic side, for two reasons. On the one hand, one could expect a "low-hanging fruit" effect by which the best locations for wind parks are built out first, and future expansions will have a lower average load factor and thus higher LCoE. On the other hand, transmission lines required to connect new wind parks directly to the steel mill could

have an extra cost. Therefore, the cost variations studied are $1\times$, $1.25\times$ and $1.5\times$ the baseline value of $c_{\text{inv}}^{\text{wind}}$.

Hydrogen purchase price. The 150 EUR/MWh assumed as baseline, corresponding to about 4.5 EUR/kg, is within the lower range of current prices for renewable H_2 currently, but it is expected that prices will go down in the future thanks to economies of scale and government subsidies (the "hydrogen economy"). Thus, the studied variations are $1\times$, $0.8\times$ and $0.6\times$ the baseline cost $c_{\text{buy}}^{H_2}$.

Electrolysers CAPEX. The investment costs for electrolysis systems have uncertainties in both directions. On the one hand, it is likely that technological innovations and economies of scale will bring down the production cost of electrolysis cells. However, it is also possible that ancillary infrastructure and adaption of gas supply systems in the furnaces (for the H_2) will induce additional investment costs. To account for all the possibilities, the studied variations are $0.5\times$, $0.75\times$, $1\times$, $1.5\times$ and $2\times$ the baseline $c_{\text{inv}}^{\text{AWE/PEM}}$ and $c_{\text{inv}}^{\text{SOEC}}$.

Taking all the possible combinations of parameter values, decarbonization routes and grid capacities, a total of 270 separate optimization runs were evaluated. It should be noted that, though here the variations are carried out separately the varied parameters may be correlated in reality. In particular, the cost of grid-purchased hydrogen can partly be shaped by upstream electricity prices, electrolyser investment costs and wind farm CAPEX. In the present study, these parameters were varied independently in order to isolate their directional influence on the optimal solution. The main results, again using LCoH as the main metric, are shown in Figure 7.

The most obvious result is that, for the price of purchasing hydrogen from the grid, there is a threshold under which the optimal solution consists of forgoing any on-site electrolysis capacity simply supplying all the H_2 through the grid, regardless of the values of the other cost parameters. The exception is the strongly constrained grid scenario, where some electrolysis capacity is still required to process excess renewable energy.

The variations in wind power CAPEX do not have a large influence on the LCoH, as they induce a reduction in wind power capacity and an increased electricity purchase from the grid, again with the exception of the strongly constrained grid. In that case, higher investment costs translate into a higher LCoH.

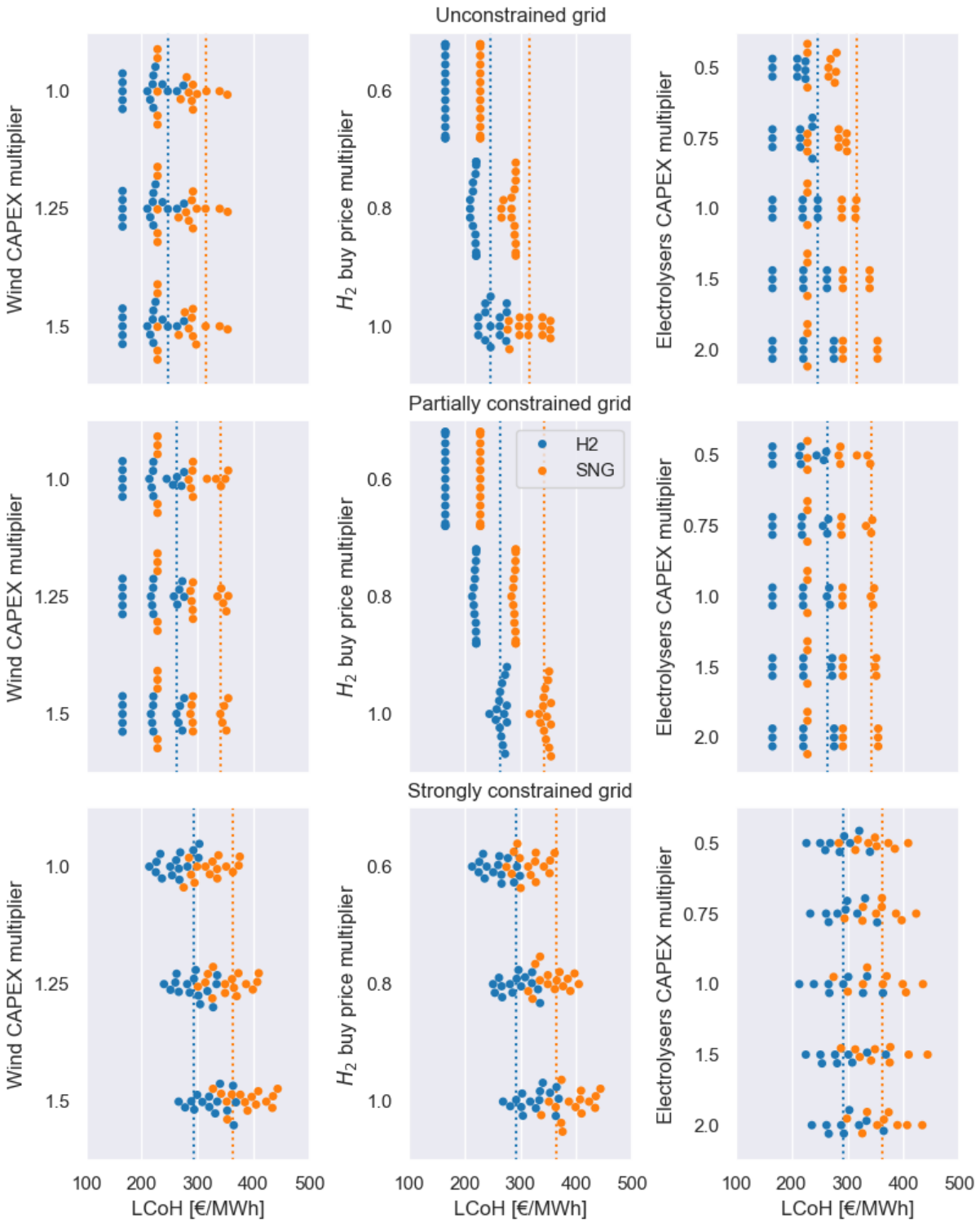

Figure 7. Distribution of LCoH generated by the 45 variations, for both routes (H_2 in blue, CC+SNG in orange). Each dots represents an individual variation. The dotted lines mark the respective baseline cost.

Finally, the variations in the specific investment cost of electrolysers seem not to have a large impact on average, but cause a larger spread in the distribution of the LCoH generated by the variations of the other parameters. However, higher investment costs do translate to an increase in LCoH while they are still below the grid purchase costs. This can be observed especially in the case of an unconstrained electricity grid connection, where increasing electrolyser costs are directly linked to an increase in LCoH.

The sensitivity analysis reveals that the response of the system is not purely gradual, but exhibits threshold-like behaviour. Most importantly, the attractiveness of on-site hydrogen production depends on the interaction between hydrogen purchase price, grid constraint and costs for renewable electricity. When hydrogen from the grid is sufficiently cheap, the model tends to forgo on-site electrolysis in favour of external supply. However, under strongly constrained grid conditions, on-site electrolysis remains valuable even at low hydrogen purchase prices because it provides a sink for excess renewable electricity. Hence, grid constraints determine whether the system shifts towards a purchase-based or production-based hydrogen supply strategy.

Implications for business

Expressed in absolute terms, the modelled LCoH rises from 109.8 EUR/MWh in the BAU case to approximately 246–292 EUR/MWh for the H2 route and 315–363 EUR/MWh for the CC+SNG route, depending on grid conditions. If product quality and heating process considerations allow for a mix of pure hydrogen and SNG, then the LCoH for the H_2 and the CC+SNG can be interpreted respectively as the lower and upper ends of the cost band for such a hybrid solution.

From an industrial perspective, these increases in levelized heat costs are not merely percentage differences but cost levels that would be difficult to absorb in a highly competitive steel market if borne by the plant alone. In other words, even the most techno-economically favourable decarbonized configurations identified here (i.e. pure-hydrogen fuel without major electricity grid constraints) do not appear to be business cases driven by direct heat-cost savings; rather, their implementation would likely depend on sufficiently strong policy support measures such as carbon pricing, CAPEX financing, OPEX subsidies, contracts for difference, or green-steel price premiums.

The results should therefore be interpreted primarily as showing the relative economic attractiveness of the modelled pathways under different infrastructure constraints, while the broader investment decision remains contingent on whether these absolute cost levels can be recovered in the market or offset by policy support. This is particularly relevant because industrial decision-makers do not choose only between hydrogen and CC+SNG, but also between these routes, partial decarbonization steps, efficiency measures, and in other cases electrification-based concepts that were not investigated in this study.

CONCLUSION

In this work, a model of a steel hot rolling mill in Austria was developed, with (i) direct combustion of green hydrogen and (ii) post-combustion carbon capture with methanation as the possible routes for decarbonizing its energy supply, and several technologies available for each subsystem. The design and operation of the energy system were simultaneously optimized using a mixed integer linear problem (MILP) formulation. Even after optimizing for minimal annualized costs, a major increase in the levelized cost of heat (LCoH) was predicted.

However, the increase in LCoH was found to be noticeably dependent on the constraints of the system. If direct combustion of green hydrogen is allowed, the cost is predicted to increase to 2.5 - 2.9 times the BAU LCoH; if synthetic natural gas (SNG) is required, then the increase is 3.2 - 3.6 times the BAU LCoH, mainly due to the extra investment costs and conversion losses of the carbon capture and methanation steps. The strictness of the limitations on the electrical grid to provide flexibility not only has a large impact on the headline LCoH, but also on the underlying configuration of the energy system.

Finally, the parameter variation analysis showed that the capital costs of wind power generation and the purchase costs of hydrogen from the gas grid also have a large influence on

the LCoH and the configuration of the system, with the investment costs of electrolysers having a comparatively minor influence. Together, the results highlight the importance of accurate modelling of the boundary conditions when predicting the costs of the energy transition, but show that optimization methods can help in revealing the cost-optimal strategies for minimizing said costs.

From a business perspective, the absolute LCoH levels suggest that, under the assumptions of this study, neither route is likely to be adopted on the basis of direct cost competitiveness alone. Rather, deployment would depend on favourable infrastructure conditions together with policy support and/or market mechanisms that reward low-carbon steel production.

Future work

The insights obtained from the present work suggest a range of refinements of the model that could prove to be interesting to investigate in future research. On the one hand, (i) the outsize impact of grid boundary conditions on the design and operation of the system calls for a more detailed modelling of the grid dynamics and the electricity and hydrogen markets, including time-dependent prices and capacities, with price fluctuations in particular having a potentially major effect on the sizing and operation of energy storages. On the other hand, (ii) more detailed modelling of operational conditions of the technologies involved in the electrolysis, carbon capture and methanation subsystems could prove useful in the context of broader feasibility studies, with more emphasis on the efficiency changes over the operating range of each technology, as well as more realistic models of energy storage technologies. Finally, the model could be expanded with (iii) additional alternative fuel possibilities (ammonia, methanol, enrichment of combustion air with oxygen produced as by-product of electrolysis) as well as with (iv) the search for optimal decarbonization pathways, i.e. intermediate solutions with partial decarbonization steps and the associated optimization of the timing of investment decisions.

Acknowledgements

This project is supported with the funds from the Climate and Energy Fund and implemented in the framework of the RTI-initiative “Flagship region Energy”.

NOMENCLATURE

Symbols

a	available surface area	[m^2]
C	C-rate of a storage	[1/h]
c	cost	[EUR/unit]
d	demand	[MW]
ef	emissions factor	[tCO_2/t]
$\mathcal{F}$	set of fuels	
I	solar irradiation	[MW/m^2]
i	interest rate	[-]
lim	part load limit	[-]
$\dot{m}$	mass flow	[kg/s]
MW_q	average thermal load of all the furnaces	[MW]
n	amortization period	[-]
p	electrical power	[MW]
$\mathcal{P}$	set of representative periods	

$\mathcal{T}$	set of time steps	
q	heat flow	[MW]
R	recovery rate	[-]
r	ratio	[-]
rq	heat fraction	[-]
SoC	state-of-charge	[MWh]
w	waste heat flow	[MW]

Greek letters

η	efficiency	[-]
λ	SoC loss	[1/h]
σ	standard deviation	
χ	conversion rate	[-]

Subscripts and superscripts

bat	battery storage
buy	purchase from external connection
BM	biomethane
cap	captured from flue gas
CH_4	methane
CO_2	carbon dioxide
elec	electrolyser
emit	emissions certificates
f	fuel
furn	furnace
hydro	hydropower
H_2	hydrogen
H_2 tank	hydrogen tank storage
in	flue gas input
inv	investment
max	maximum allowed value
meth	methanation
min	minimum allowed value
NG	natural gas
p	representative period
peak	maximum value of the series
power	grid electricity
pr	product
ren	renewable energies
sell	feed-in to external connection
slip	not captured from flue gas
t	time step
wind	wind power
>150	temperature over 150°C

Abbreviations

AS	Amine Scrubber
ASHP	Amine Scrubber with Heat Pump
AWE	Alkaline Water Electrolysis
BAU	Business-As-Usual
CAPEX	Capital Expenditures

CC	Carbon Capture
CCU	Carbon Capture and Utilization
HTHP	High-Temperature heat pump
LCoE	Levelized Cost of Energy
LCoH	Levelized Cost of Heat
LF	Load Factor
lgSNG	low-grade Synthetic Natural Gas
LHV	Lower Heating Value
MILP	Mixed-Integer Linear Programming
OPEX	Operational Expenditures
OSM	One-Stage Methanation
PEM	Proton Exchange Membrane
PSA	Pressure Swing Adsorption
PV	PhotoVoltaic
SNG	Synthetic Natural Gas
SOEC	Solid Oxide Electrolysis Cell
TRL	Technology Readiness Level

References

Journal articles

4. Leicher, J., Giese, A., and Wieland, C., Electrification or Hydrogen? The Challenge of Decarbonizing Industrial (High-Temperature) Process Heat, *J*, Vol.7, No. 4, pp. 439–456, 2024, doi: 10.3390/j7040026.
6. Schmitz, N., Sankowski, L., Kaiser, F., Schwotzer, C., Echterhof, T., and Pfeifer, H., Towards CO2-neutral process heat generation for continuous reheating furnaces in steel hot rolling mills – A case study, *Energy*, Vol.224, p. 120155, 2021, doi: 10.1016/j.energy.2021.120155.
8. Della Rocca, A., Astesiano, D., and Malfa, E., Rolling mill decarbonization: Tenova SmartBurners with 100% hydrogen, *Matériaux & Techniques*, Vol.109, 3-4, p. 309, 2021, doi: 10.1051/mattech/2022012.
9. Ameli, H., Strbac, G., Pudjianto, D., and Ameli, M. T., A Review of the Role of Hydrogen in the Heat Decarbonization of Future Energy Systems: Insights and Perspectives, *Energies*, Vol.17, No. 7, p. 1688, 2024, doi: 10.3390/en17071688.
10. Airaksinen, S., Haapakangas, J., Gyakwaa, F., Heikkinen, E.-P., and Fabritius, T., Utilization of hydrogen fuel in reheating furnace and its effect on oxide scale formation of low-carbon steels, *International Journal of Hydrogen Energy*, Vol.140, pp. 1212–1220, 2025, doi: 10.1016/j.ijhydene.2024.11.230.
11. Emel'yanov, A. V., Lube, I. I., Kuznetsov, V. I., and Levchenko, D. A., Scale Formation Minimization on Internal Surface of Seamless Hot-Rolled Pipes, *Steel Transl.*, Vol.50, No. 5, pp. 340–346, 2020, doi: 10.3103/S0967091220050046.
12. Haapakangas, J., Airaksinen, S., Heikkinen, E.-P., and Fabritius, T., Oxidation of Carbon Steels in Novel Reheating Conditions: Changes to Oxidation Kinetics, *Metall Mater Trans B*, Vol.56, No. 4, pp. 3762–3773, 2025, doi: 10.1007/s11663-025-03588-7.
13. Haapakangas, J., Riikonen, S., Airaksinen, S., Heikkinen, E.-P., and Fabritius, T., Oxide Scale Formation on Low-Carbon Steels in Future Reheating Conditions, *Metals*, Vol.14, No. 2, p. 189, 2024, doi: 10.3390/met14020189.
15. Yamamoto, S., Sayama, S., Kunitomi, S., Ogasawara, K., and Baba, N., Demonstration of a high-efficiency carbon dioxide capture and methanation system with heat/material integration for power-to-gas and zero carbon dioxide emissions in flue gasses, *International Journal of Greenhouse Gas Control*, Vol.114, p. 103584, 2022, doi: 10.1016/j.ijggc.2022.103584.

16. Giglio, E., Lanzini, A., Santarelli, M., and Leone, P., Synthetic natural gas via integrated high-temperature electrolysis and methanation: Part I—Energy performance, *Journal of Energy Storage*, Vol.1, pp. 22–37, 2015, doi: 10.1016/j.est.2015.04.002.
17. Zabik, G., Birkelbach, F., and Hofmann, R., Hydrogen and Synthetic Natural Gas for decarbonizing steel hot rolling mills: Economic viability under dynamic electricity pricing, *Energy Conversion and Management*, Vol.341, p. 119912, 2025, doi: 10.1016/j.enconman.2025.119912.
18. Miserocchi, L. and Franco, A., Techno-Economic Assessment of Electrification and Hydrogen Pathways for Optimal Solar Integration in the Glass Industry, *Solar*, Vol.5, No. 3, p. 35, 2025, doi: 10.3390/solar5030035.
19. Guo, Z. and Zhou, S., Modeling and Multi-Stage Planning of Cement-IIES Considering Carbon-Green Certificate Trading, *Processes*, Vol.11, No. 4, p. 1219, 2023, doi: 10.3390/pr11041219.
20. Tiggeloven, J. L., Faaij, A. P. C., Kramer, G. J., and Gazzani, M., Optimizing Emissions Reduction in Ammonia–Ethylene Chemical Clusters: Synergistic Integration of Electrification, Carbon Capture, and Hydrogen, *Ind. Eng. Chem. Res.*, Vol.64, No. 8, pp. 4479–4497, 2025, doi: 10.1021/acs.iecr.4c03817.
35. Sebbahi, S., Nabil, N., Alaoui-Belghiti, A., Laasri, S., Rachidi, S., and Hajjaji, A., Assessment of the three most developed water electrolysis technologies: Alkaline Water Electrolysis, Proton Exchange Membrane and Solid-Oxide Electrolysis, *Materials Today: Proceedings*, Vol.66, pp. 140–145, 2022, doi: 10.1016/j.matpr.2022.04.264.
41. Bukar, A. M. and Asif, M., Technology readiness level assessment of carbon capture and storage technologies, *Renewable and Sustainable Energy Reviews*, Vol.200, p. 114578, 2024, doi: 10.1016/j.rser.2024.114578.
43. Riboldi, L. and Bolland, O., Overview on Pressure Swing Adsorption (PSA) as CO2 Capture Technology: State-of-the-Art, Limits and Potentials, *Energy Procedia*, Vol.114, pp. 2390–2400, 2017, doi: 10.1016/j.egypro.2017.03.1385.
44. Susarla, N. *et al.,* Energy and cost estimates for capturing CO2 from a dry flue gas using pressure/vacuum swing adsorption, *Chemical Engineering Research and Design*, Vol.102, pp. 354–367, 2015, doi: 10.1016/j.cherd.2015.06.033.
45. Subraveti, S. G., Roussanaly, S., Anantharaman, R., Riboldi, L., and Rajendran, A., How much can novel solid sorbents reduce the cost of post-combustion CO2 capture? A techno-economic investigation on the cost limits of pressure–vacuum swing adsorption, *Applied Energy*, Vol.306, p. 117955, 2022, doi: 10.1016/j.apenergy.2021.117955.
46. Husebye, J., Brunsvold, A. L., Roussanaly, S., and Zhang, X., Techno Economic Evaluation of Amine based CO2 Capture: Impact of CO2 Concentration and Steam Supply, *Energy Procedia*, Vol.23, pp. 381–390, 2012, doi: 10.1016/j.egypro.2012.06.053.
47. Rönsch, S. *et al.,* Review on methanation – From fundamentals to current projects, *Fuel*, Vol.166, pp. 276–296, 2016, doi: 10.1016/j.fuel.2015.10.111.
48. Tommasi, M., Degerli, S. N., Ramis, G., and Rossetti, I., Advancements in CO2 methanation: A comprehensive review of catalysis, reactor design and process optimization, *Chemical Engineering Research and Design*, Vol.201, pp. 457–482, 2024, doi: 10.1016/j.cherd.2023.11.060.

Theses and dissertations

21. Löffler, S., Transformation of a Steel Rolling Plant : Identification of Decarbonisation Pathways using MILP, *PhD Thesis,* School of Industrial Engineering and Management, KTH Royal Institute of Technology, Stockholm, Sweden, 2024, https://www.diva-portal.org/smash/record.jsf?pid=diva2:1901069.

Proceedings

14. Şahin, A. Y., Işikgül, A., Işikgül, O., Imer, S. T., and Yaşacan, D., Investigation of Decarburization of Spring Steel During Hot Rolling, *AISTech 2025 Conference Proceedings*, Nashville, USA, 2025.
42. Wilk, V., Leibetseder, D., Zauner, C., Rath, A., and Schwaiger, M., Improving Energy Efficiency of Carbon Capture Processes with Heat Pumps, *3rd Sustainable Energy Conference Proceedings*, Graz, Austria, 2024.

Reports

1. World Steel Association, SteelFacts, 2024, https://worldsteel.org/wp-content/uploads/steelFacts-2024.pdf.
2. World Steel Association, World Steel in Figures 2025, 2025, https://worldsteel.org/wp-content/uploads/World-Steel-in-Figures-2025-3.pdf.
3. International Energy Agency (IEA), Tracking industrial energy efficiency and CO2 emissions: *In support of the G8 plan of action*. Paris: OECD Publishing, 2007.
5. Pardo, N., Moya, J., and Vatopoulos, K., Prospective scenarios on energy efficiency and CO2 emissions in the EU iron & steel industry: Re-edition, European Commission, Luxembourg, 2015.
24. Wlcek, B. *et al.,* Marktbericht 2023 (in German, Market Report 2023), Renewable Gases Service Point, 2023, https://www.erneuerbaresgas.at/jart/prj3/erneuerbare_gase/data/uploads/SEG%20Marktbericht%202023.pdf.
25. Kutz, C. *et al.,* Potenzialstudie Grüne Gase: Analyse und Bewertung der Potenziale Grüner Gase in der Innovationsregion Mitteldeutschland (in German, Potential Study Renewable Gases: Analysis and Evaluation of the Potential of Green Gases in the Innovation Region Middle Germany), Sep. 2022, https://transformationsregion-mitteldeutschland.com/wp-content/uploads/2022/05/2022-02-09_Potenzialstudie_Gruene_Gase_Materialband_final.pdf.
27. Kathan, J. *et al.,* Importmöglichkeiten für erneuerbaren Wasserstoff (in German, Import Possibilities for Renewable Hydrogen), Austrian Federal Ministry for Climate Protection, Environment, Energy, Mobility, Innovation and Technology, 2022, https://www.bmwet.gv.at/dam/jcr:26f6c51d-2c46-49df-9701-f5cedbbc3dcc/SGP-22413_Endbericht_Importmoeglichkeiten-Erneuerbarer-Wasserstoff_final.pdf.
30. Altaghlibi, M. and Gentile, G., Scenarios shaping EU ETS prices, 2026, https://www.abnamro.com/research/en/our-research/esg-economist-scenarios-shaping-eu-ets-prices.
31. Jaksch-Fliegenschnee, M., Wonisch, P., and Krenn, A., IEA Wind TCP Austria 2022, International Energy Agency, 2023.
32. Kost, C., Müller, P., Sepúlveda Schweiger, J., Fluri, V., and Thomsen, J., Study: Levelized Cost of Electricity- Renewable Energy Technologies, Fraunhofer ISE, 2024.
33. Fechner, H., National Survey Report of PV Power Applications in Austria 2023, International Energy Agency, 2024, https://iea-pvps.org/national_survey/national-survey-report-of-pv-power-applications-in-austria-2023/.
34. Philipps, S. and Warmuth, W., Photovoltaics Report, Fraunhofer ISE, 2025, https://www.ise.fraunhofer.de/content/dam/ise/de/documents/publications/studies/Photovoltaics-Report.pdf.
36. Holst, M., Aschbrenner, S., Smolinka, T., Voglstätter, C., and Grimm, G., Cost Forecast for Low-Temperature Electrolysis - Technology Driven Bottom-Up Prognosis for PEM and Alkaline Water Electrolysis Systems, Fraunhofer ISE, 2021.
37. Energy Sector Management Assistance Program, Electrolyzers for Hydrogen Production: Technical and Economic Characteristics Executive Summary, World Bank Group, 2026.

38. van 't Noordende, H., van Berkel, F., and Stodolny, M., Next Level Solid Oxide Electrolysis: Upscaling potential and techno-economical evaluation for 3 industrial use cases, Institute for Sustainable Process Technology, Amersfoort, the Netherlands, 2023.
50. Bielewski, M. *et al.,* Battery technology in the European Union2024 Status report on technology development, trends, value chains and markets, Publications Office of the European Union, Luxembourg, 2024.
51. Gardiner, M., DOE Hydrogen and Fuel Cells Program Record 9013Energy requirements for hydrogen gas compression and liquefaction as related to vehicle storage needs, United States Department of Energy, 2009.

Online resources

7. Häggström, G., Electrification of reheating furnaces: state of the art and future research needs. Algarve, Portugal, 2024, https://dissheat.eu/wp-content/uploads/2024/04/INFUB14_haggstrom_Electrification-of-reheating-furnaces.pdf.
22. Austrian Power Grid, APG's Future Grid Puts Supply-Secure Energy Transition on the Fast Track, https://www.apg.at/en/news-press/apgs-future-grid-puts-supply-secure-energy-transition-on-the-fast-track/, [Accessed: 11-March-2026].
23. Statistik Austria, Energy prices, taxes, https://www.statistik.at/en/statistics/energy-and-environment/energy/energy-prices-taxes, [Accessed: 11-March-2026].
26. International Energy Agency, Real-Time Electricity Tracker, https://www.iea.org/data-and-statistics/data-tools/real-time-electricity-tracker?from=2015-1-1&to=2024-12-31&category=price&country=AUT, [Accessed: 11-March-2026].
28. Ministerialentwurf Erneuerbares-Gas-Gesetz (in German, Renewable Gas Act Ministerial Draft), https://www.parlament.gv.at/gegenstand/XXVII/ME/251.
29. Austrian Energy Agency, Emissionspreisindex (in German, Emissions Price Index), https://www.energyagency.at/fakten/emissionspreisindex, [Accessed: 11-March-2026].
39. Siemens Energy, Silyzer 300: The next paradigm of PEM electrolysis, https://p3.aprimocdn.net/siemensenergy/3baa4ffa-f1f1-422f-a770-b08300c0f2b0/Datasheet-Silyzer300-pdf_Original%20file.pdf, [Accessed: 11-March-2026].
40. Sunfire SE, Sunfire-HyLink SOEC, http://backend.sunfire.de/wp-content/uploads/2024/10/Sunfire_Fact-Sheet_SOEC_EN_digital.pdf, [Accessed: 11-March-2026].
49. Chint Power Systems, 5 MWh Battery Energy Storage System for North America, https://www.chintpowersystems.com/wp-content/uploads/2024/03/CPS-5-MWh-BESS-Datasheet-3-15-2024.pdf.

APPENDIX

As solving the MILP problem for an entire year is computationally infeasible, a balance has been sought between robust results that allow for drawing meaningful conclusions and fast computation that enables iteration over many scenarios and sets of parameters. In order to find this "sweet spot", one of the scenarios (SNG route with partially constrained grid regime) was configured with either 1, 2, 4, 8, 16, 22, or 32 representative days. For each number of representative days, the optimization was run 13 separate times, each time using a different subset of the whole year chosen randomly without replacement. The two metrics calculated for each number of days from these validation runs are i) the standard deviation in the total value of the objective function, as an increase in total costs relative to the business-as-usual scenario; and ii) the mean computation time on the same machine. The Pareto front in Figure 8 shows that 22 days (one-sixteenth of the year) strikes a good balance between the robustness of the results (low spread in objective function value) and computational efficiency (quick runtime).

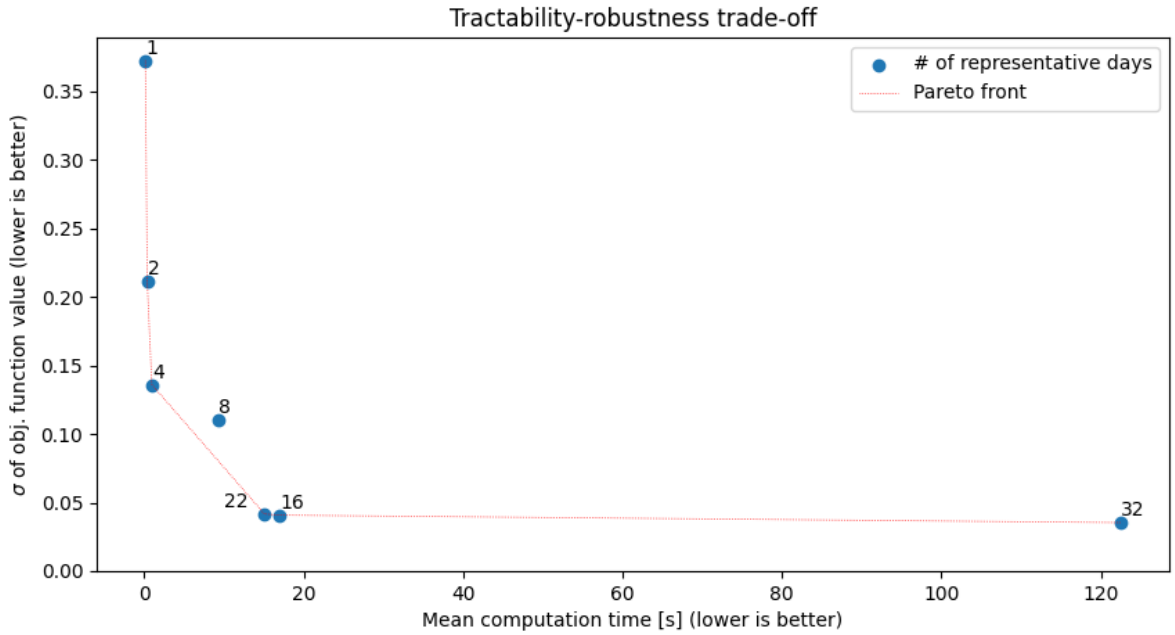

Figure 8. Result of validation runs for the SNG scenario with partially constrained grid. Increasing the number of representative days initially produces a large improvement in robustness in the 10-20 days region before running into diminishing returns past 22 days.